Research Repository UCD

Title	Geometric and kinematic controls on the internal structure of a large normal fault in massive limestones : the Maghlaq Fault, Malta
Authors(s)	Bonson, Chris G., Childs, Conrad, Walsh, John J., Schöpfer, Martin P. J., Carboni, Vincent
Publication date	2007-02
Publication information	Bonson, Chris G., Conrad Childs, John J. Walsh, Martin P. J. Schöpfer, and Vincent Carboni. "Geometric and Kinematic Controls on the Internal Structure of a Large Normal Fault in Massive Limestones : The Maghlaq Fault, Malta" 29, no. 2 (February, 2007).
Publisher	Elsevier
Item record/more information	http://hdl.handle.net/10197/3024
Publisher's statement	This is the author's version of a work that was accepted for publication in Journal of Structural Geology. Changes resulting from the publishing process, such as peer review, editing, corrections, structural formatting, and other quality control mechanisms may not be reflected in this document. Changes may have been made to this work since it was submitted for publication. A definitive version was subsequently published in Journal of Structural Geology Volume 29, Issue 2, February 2007, Pages 336-354 DOI#:10.1016/j.jsg.2006.06.016.
Publisher's version (DOI)	10.1016/j.jsg.2006.06.016

Downloaded 2024-04-19 02:29:54

The UCD community has made this article openly available. Please share how this access benefits you. Your story matters! (@ucd_oa)

© Some rights reserved. For more information

Geometric and kinematic controls on the internal structure of a large normal fault in massive limestones: the Maghlaq Fault, Malta.

C.G. Bonson*[1], C. Childs, J.J. Walsh, M.P.J. Schöpfer and V. Carboni[2]

Fault Analysis Group, School of Geological Sciences, University College Dublin, Belfield, Dublin 4, Ireland.

[1]Present address: SRK Consulting (Canada), Suite 800, 1066 West Hastings St., Vancouver, British Columbia, V6E 3X2. Canada.

[2]Present address: Alcan Inc., 1188 Sherbrooke St. West, Montreal, Quebec, H3A 3G2. Canada.

Corresponding author: John Walsh

Email: fault@fag.ucd.ie

Tel: +353 1 716 2606

Fax: +353 1 716 2607

No. of words: 11469

No. of figures: 15

ABSTRACT

The Maghlaq Fault is a large, left-stepping normal fault (displacement >210m) cutting the Oligo-Miocene pre- to syn-rift carbonates of SW Malta. Two principal slip zones separate the deformed rocks of the fault zone from the undeformed wall rocks. Fault rocks derived from fully lithified, pre- to early syn-rift sediments comprise relatively continuous fine-grained veneers of cataclasite and localised fault-bound lenses of wall rock, occurring over a range of scales, which are commonly brecciated. The lenses result from the linkage of slip surfaces, the inclusion of asperities and the formation of Riedel shears within the fault zone. In contrast, fault rock incorporated from unlithified syn-rift sediments comprise relatively continuous veils of rock that deformed in a ductile manner. Anomalously thick parts of the fault zone with highly complex structure and content are associated with breached relay zones, branch-lines and bends; these structures represent progressive stages of fault segment linkage. The progressive evolution and bypassing of fault zone complexities to form a smoother and more continuous active fault surface, results in complex fault rock distributions within the fault zone. Segment linkage structures have high fracture densities which combined with their significant vertical extents suggest they are potentially important up-fault fluid flow conduits.

200 WORDS

Keywords: branch-line, fault zone, fluid flow, relay, segment linkage.

1. Introduction

An appreciation of the spatial heterogeneity of fault zones is a prerequisite for constructing conceptual models of fault zone structure and is fundamental to an understanding of the mechanical and hydrological behaviour of faults. Despite the importance of outcrop-scale observational constraints, few detailed studies of the 2D and 3D structure of normal fault zones within carbonate successions dominated by massive limestones are available within the published literature. This paucity of data is partly attributable to the difficulty of identifying and examining faults within thick and homogeneous limestone sequences and to the often relatively poor preservation potential of faults in limestones, sometimes arising from the operation of karstic processes. In this article, we provide a detailed description of the internal architecture of the Maghlaq Fault, a normal fault zone in southwest Malta, which offsets a Tertiary pre- to syn-rift carbonate succession by a minimum of 210m. There is near-continuous exposure of the footwall to the Maghlaq Fault over a 4km long coastal outcrop. The hangingwall is preserved for 2.5km and coastal inlets provide numerous cross-sections through the fault zone. Detailed field mapping on to aerial photographs was carried out at 1:4000 and, locally, at 1:200 scales to characterise the heterogeneity in structure and content of the Maghlaq Fault Zone.

The tectonic setting and stratigraphic framework of the study area are outlined in the following section. A summary of the main characteristics of the Maghlaq Fault is then followed by a consideration of the along strike variability of the basic structure and content of the fault zone and the nature of fault rocks. Building on the description of the basic fault zone structure, we then describe several large-scale fault complexities which represent elements of anomalous fault zone structure; namely relay zones, branch-lines and bends. These structures are considered in terms of the fault zone processes active during growth of the Maghlaq Fault. Finally, we discuss

the structure of the Maghlaq Fault in terms of the generic permeability structure of fault zones in carbonate successions and speculate about the potential implications for subsurface fluid flow.

2. Geology of the Maghlaq Fault

2.1. Tectonic setting

The Maltese Islands are situated on the northern flank of the WNW-ESE striking Pantelleria Rift system (Reuther and Eisbacher, 1985), also known as the Strait of Sicily Rift (Finetti et al. 1984; Cello et al. 1985). The Pantelleria Rift is an elongate fault-controlled trough within the foreland of the Sicilian Apennine-Maghrebian thrust and fold belt (Hill and Hayward, 1988; Pedley, 1990) (Fig. 1). The largest faults in the Pantelleria Rift accommodate throws of >2km (Fig. 2) and are associated with the development of a stepped seafloor topography and the opening of three exceptionally deep troughs: the Malta Trough, the Linosa Trough and the Pantelleria Trough, in which the seafloor bathymetry exceeds 1km in depth (Jongsma et al. 1985). The major development of the Pantellaria Rift took place during Plio-Quaternary times, when displacement rates far outstripped sedimentation rates within the central parts of the basin (Dart et al. 1993). The uplift of the northern rift flank (i.e., the present-day Maltese Archipelago) from the Miocene onwards, together with a falling sea-level, resulted in the emergence of the islands during early Messinian times (Pedley, 1987a).

The Maghlaq Fault has a maximum displacement of >210m, making it the largest displacement fault outcropping in the archipelago. In contrast to the majority of faults in Malta which strike ENE-WSW, the Maghlaq Fault strikes WNW-ESE (Fig. 2) and is the only major fault of the Maltese Islands with a Pantelleria Rift trend

(Figs 1 and 2). Although the two sets of faults are nearly orthogonal, analysis of fault-related changes in sediment thickness, imaged on offshore 2D seismic data, reveals a shared four stage tectono-sedimentary history for the Miocene-Quaternary Periods (Fig. 3), as follows: (a) pre-rift phase (>21 Ma); (b) early syn-rift phase (21-6 Ma) characterised by minor fault-controlled thickness changes and the development of neptunian dykes; (c) late syn-rift phase (<5 Ma) during which major fault growth took place and localised basin depocentres and areas of non-deposition evolved; and (d) post-rift phase (probably <1.5 Ma; Dart et al. 1993).

2.2. Stratigraphic Framework

The stratigraphy of the Maltese Graben system consists of five main litho-stratigraphic units that represent a relatively simple Oligo-Miocene pre- to syn-rift succession (Fig. 3; Pedley, 1990; Dart et al. 1993). The nature of the individual formations, their moderate thickness changes and lateral variations across the islands have been documented by previous workers (e.g. Bennett, 1980; Pedley, 1978; 1987a; 1987b; 1990; 1996; 1998; Pedley et al. 1976; Pedley and Bennett, 1985). At the base of the exposed succession are the Oligocene (Chattian) Lower Coralline Limestones, which can be up to 1000m thick (Pedley et al. 1976), although only the uppermost 140m are exposed in the Maltese Archipelago (Fig. 3). The outcropping limestones predominantly comprise pale yellow biomicrites at their lowermost exposures, conformably overlain by massively bedded coralline algal limestones, representing sedimentation in restricted gulf to open-marine conditions (Pedley 1978). Near the top of the succession, deposition in a shallow marine shoal environment gave rise to cross-bedding of coarse bioclastic limestones (Pedley et al. 1976).

Overlying the Lower Coralline Limestone is the Aquitanian to Serravallian age Globigerina Limestone Formation (Fig. 3), a relatively uniform succession of yellow to grey-white coloured, biomicritic wackestones and marls that may attain thicknesses of >200m. These limestones largely consist of massive units of poor-moderately consolidated planktonic foraminifera (globigerina) and pteropods (Pedley, 1978) and represent a deepening to outer shelf conditions (Bennett, 1980). Occasional marker horizons occur in the form of brown phosphoritic conglomeratic layers (<0.7m in thickness) which overlay well-developed hardgrounds (Pedley and Bennett, 1985).

A major lithological transition occurs at the top of the Globigerina Limestone, where biomicrites grade over 1m into globigerinid marls at the base of the Blue Clay Formation (Fig. 3). On Malta, the Blue Clay consists of up to 65m of pale grey-green banded clays which predominantly consist of kaolinite and glauconite, with <30% carbonate material (Pedley et al. 1976; Pedley and Bennett, 1985). The Blue Clay is interpreted as sediment deposited within an open muddy marine environment with water depths of about 150m during the mid- to late Serravalian (Pedley et al. 1976). Capping the Blue Clay, is a very poorly cemented, dark blue-green bioclastic glauconitic limestone known as the Greensand Formation (Pedley, 1978), which is rarely greater than 1m thick throughout Malta. The presence of intense bioturbation within this Tortonian age unit indicates that it was deposited in shallow marine conditions (Pedley et al. 1976; Dart et al. 1993).

The uppermost outcropping unit of the Maltese stratigraphy is the Late Tortonian to Messinian age Upper Coralline Limestone Formation (Fig. 3). The succession comprises three depositional units which show a transition from coralline algal biostrome facies at the base to coral and algal patch reefs and finally to platform and slope facies at the top of the formation (Pedley, 1987b; Bosence and Pedley;

144 1982). These represent the principal syn-faulting depositional packages which show
145 marked changes in both facies-type and thickness across the fault (Dart et al. 1993).
146 The flat-lying footwall outcrops predominantly consist of massive Lower
147 Coralline Limestone, which varies from a hard, low porosity-low permeability
148 mudstone (Maghlaq Member), to bioclastic wackestones and packstones (Xlendi and
149 Attard Members; Pedley 1993). Inland, the Lower Coralline Limestone is capped by
150 the Globigerina Limestone, and in sporadic flat-topped hills the remainder of the
151 Miocene strata is preserved. Local stratigraphic thickness determinations derived from
152 the footwall succession are given in Fig. 3.
153 The hangingwall of the Maghlaq Fault, exposed over the westernmost 2.5km
154 of the fault outcrops, predominantly consists of well-bedded calciturbidites and inter-
155 sand shoals belonging to the Upper Coralline Limestone (Dart, 1991). The absence of
156 exposures of pre-rift strata in the hangingwall precludes the determination of absolute
157 displacements. However, on the basis of stratigraphic thicknesses within the direct
158 footwall of the fault local to Ghar Lapsi, a minimum displacement of 210m can be
159 calculated (Figs 3 and 4).
160
161 *2.3. Timing and conditions of faulting*
162 Using fault-related stratigraphic thickness changes identified on 2-D seismic
163 data, Dart et al. (1993) proposed two periods of normal fault activity in the Pantelleria
164 Rift: (a) an early syn-rift phase (21-6 Ma); and (b) a late syn-rift phase (<5 Ma; Fig.
165 3). The early and late syn-rift sediment packages in the Pantellaria Rift are
166 approximately 4 and 9 times thicker, respectively, than onshore Malta. Across the
167 Maghlaq Fault, sequence thickening and associated variations in sedimentary facies of
168 the Upper Coralline Limestone Formation reflect Tortonian-Lower Messinian age

displacements of the late syn-rift phase (Dart et al. 1993; Pedley, 1987b). Burial of the underlying lithologies in the hangingwall, precludes the confirmation of a probable early syn-rift movement history.

The most recent age for significant displacements on the Maghlaq Fault is given by late Pleistocene-Holocene age alluvial fanglomerates (Pedley, 1993), which overlie an erosion surface at several places along the fault scarp. Where the fans cross the fault, they are offset by a few tens of centimetres. Neotectonic fault movements along the Maghlaq Fault or other faults in the Maltese Archipelago have not been reported.

Although thick post-Miocene marine successions are found offshore (Dart et al. 1993), Pliocene sediments are absent onshore, and thin, patchy Quaternary marine deposits are restricted to the northwest and southeast extremes of Malta. The presence of caves and karstic surface depressions containing Pleistocene bones of land-dwelling mammals (Pedley et al. 1976) and the lack of significant sediment thicknesses suggest that, similar to the Hyblean Mountains of SE Sicily, post-Messinian Malta remained emergent to the present day (Martyn Pedley, written communication, 2002). Based on the total thickness of the exposed footwall stratigraphy above the level of the present-day outcrop of the Maghlaq Fault (Fig. 3), the burial depth during the Miocene is therefore unlikely to have been more than 300m.

Previous studies have highlighted the importance of pressure solution as a deformation mechanism in fault zones in limestones, particularly during fault nucleation (Odonne and Massonat, 1992; Willemse et al. 1997; Peacock et al. 1998; Graham et al. 2003). The lack of any discernible structures indicative of pressure

193 solution processes (e.g. stylolites and veins) along the Maghlaq Fault is attributed to
194 faulting at a very shallow crustal level.
195
196 **3. Main characteristics of the Maghlaq Fault**
197 The overall geometry of the Maghlaq Fault is that of a left-stepping, en-
198 echelon normal fault array. Relatively straight, 1-2 km long fault segments, which
199 strike WNW-ESE and dip 60º-75º SSW, have orthogonal separations of 50-400m
200 (Fig. 4). These segments are linked (or in some cases are conjectured to link offshore)
201 by short sections of the fault that strike approximately E-W or ENE-WSW, forming
202 fault bends at Ix-Xaqqa, Ras Hanzir and Ras il-Hamrija (Fig. 4).
203 The Maghlaq Fault Zone, *sensu stricto,* is a clearly defined zone of intensely
204 deformed rocks, 5-40m wide, separated from less deformed hangingwall and footwall
205 rocks by a pair of major slip zones. The hangingwall bounding slip zone is marked by
206 strongly sheared Upper Coralline Limestone sediments, ranging 2-10m in thickness,
207 containing a fault-parallel planar foliation defined by elongate ribbons of fine and
208 coarse-grained sediment. The footwall fault zone boundary is defined by planar,
209 polished Lower Coralline Limestone slip surfaces, coated with a veneer of fine-
210 grained cataclasite (Sibson 1977). Movement striations, corrugations and polish marks
211 on the footwall slip surface and on internal fault-bound lenses range in pitch from 75º
212 ESE to perfectly dip-parallel, indicating that the normal displacement has a minor
213 sinistral component.
214 Between Ix-Xaqqa and Ghar Lapsi, the hangingwall bedding dips 10-20ºS and
215 is cut by several antithetic and synthetic faults (Fig. 5a; section A-A'). Antithetic
216 faults terminate into a distributed zone of ductile deformation where they approach
217 the main fault zone. This geometry is consistent with the Upper Coralline Limestone

being unlithified, or partially lithified, at the time of deformation (Maltman, 1994). Towards the east, the dip of the hangingwall bedding steepens to about 40ºS, due to normal drag along the fault. This steepening is accompanied by increasing structural complexity of the hangingwall. At In-Neffiet (Fig. 4), the sediments are locally overturned, dipping sub-vertically towards the north and are displaced by a north-dipping low-angle thrust fault. Similar deformation has been recorded in the hangingwalls of growth faults in the Gulf of Suez rift (Gawthorpe et al. 1997). The presence of a recumbent fold in moderately inclined hangingwall calci-turbidites at Il-Miqtub (Fig. 4) suggests that drag along the fault resulted in a southward dipping topography, causing local gravity collapse and slumping of unconsolidated Upper Coralline Limestone sediments.

4. Fault rock types and distributions

To record the along strike variation in the internal architecture of the fault zone, sections were constructed at 9 stations by projecting data from cliff sections and exposures within gullies over strike-parallel distances of 1-100m on to vertical planes (Fig. 5). The locations of sections (Fig. 5a) allow the principal characteristics and internal variability of the fault zone to be assessed on a lateral scale of tens to hundreds of metres.

Fault rocks derived from each offset stratigraphic unit, from the Lower Coralline Limestone to the Upper Coralline Limestone, are observed along the studied outcrops. The different fault rocks are stacked in the stratigraphic order of their parent wall rocks, although the fault rock stratigraphy is rarely complete. Fault rocks occur mainly as extensive sheets covering large parts of the fault surface or occur within, or associated with, well-defined lenses. The type and distribution of fault rock varies

between the different source lithologies. Here we describe the character, typical occurrence and variability in thickness of the fault rock components derived from each of the four offset units in stratigraphic order. The spatial variation of the different fault rock components is illustrated schematically in Fig. 6. The largest fault zone thickness variabilities can be related to large scale (>100m) irregularities in the fault trace which are described in a later section.

4.1. Lower Coralline Limestone

The immediate footwall of the Maghlaq Fault is cut by mm-scale offset deformation bands oriented sub-parallel to the main fault (Fig. 7a). The deformation bands occur in arrays extending up to 15m into the footwall, with the highest frequencies of bands occurring closest to the principal fault. Analysis of the spacings of the deformation bands indicates that they are uniformly distributed, with mean frequencies of 6-17 per metre. The arrays contain clusters 0.1-0.2m wide, where deformation band frequencies reach 55 per metre. The ±20º variability in the strike of the deformation bands, coupled with their close spacing, results in a high degree of connectivity.

Individual deformation bands are generally <1.5mm wide and are defined by a zone of comminuted angular bioclasts within a micritic matrix, bounded on one or both sides by a connected system of discrete shears (Fig. 7a)., Cataclasis of the moderately porous Lower Coralline Limestone results in a decrease of the porosity of the limestone within the deformation bands, in the same manner as occurs within deformation bands in high porosity sandstones (Aydin and Johnson, 1978).

Deformation band arrays are absent or very poorly developed over significant areas of exposed limestone in the direct footwall of the Maghlaq Fault. The widest

arrays occur at Il-Miqtub (≥15m wide; Fig. 5a; section F-F') and Ras il-Hamrija (15m wide; Fig. 5a; section G-G'), where a large lens of Lower Coralline Limestone is bounded by two principal traces of the Maghlaq Fault (Fig. 4) that are relatively closely spaced (approximately 60 and 85m respectively). These wide deformation band arrays reflect the higher internal strains of the lens, which is also shown by a small rotation (<5º) of bedding in sympathy to the fault displacement (i.e. towards the SSW).

The footwall slip surface of the Maghlaq Fault is a pronounced, and frequently cliff-forming, polished and striated surface (Fig. 7b). Beneath the fault surface is a hard, very fine-grained, low-porosity cataclasite up to 30mm thick that has a sharp contact with the parent rock (Fig. 7c) Fault breccia, as defined by Sibson (1977), is rare within the fault zone but occurs particularly at branch-lines between slip surfaces (Fig. 6). The breccias are moderately-strongly cohesive and range from coarse breccias, containing cm-scale highly angular clasts (Fig. 7d), to microbreccias containing sub-angular to sub-rounded fragments. All breccias exhibit a moderate to high degree of porosity.

Lens-shaped slivers of intact Lower Coralline Limestone occur within the fault zone (Figs. 6 and 8a). The preserved lenses, which have strike-parallel lengths of 3m to 40m, are derived from the footwall. Limited measurements of the dimensions of these lenses from the Maghlaq Fault and smaller faults elsewhere in Malta indicate that the average lens length is about11 times the thickness, and the dip dimensions are 1.2 to 2.2 times the length.

Moderate internal deformation of the lenses, principally that of progressive flattening and elongation parallel to fault dip, is accommodated by steep, sometimes oversteepened (and therefore thrust-like), Riedel shears (Fig. 8b). Additionally,

293 localised internal shear strain, in sympathy with the fault displacements, is
294 accommodated by intense microfracturing, generally oriented parallel and
295 perpendicular to the slip direction. This type of deformation has only been detected in
296 lenses containing rare less-competent beds within the Lower Coralline Limestone.
297 Lenses become brecciated or are intensely fractured by minor faults, where they taper
298 to a thickness of a few decimetres at their fringes (Fig. 8c). The lateral fringes of the
299 lenses, which represent minor branch-lines within the fault system where slip surfaces
300 coalesce, are generally oriented parallel or sub-parallel to the slip direction (Fig. 8a
301 and 8c).

302 For a given field measurement of the total fault zone thickness, the thickness
303 of individual lithological components can be compared to a *predicted* thickness, T_{LITH},
304 based on the assumptions that all lithologies displaced past a point contribute equally
305 to the fault zone and displacement is constant along the fault trace, as depicted in Fig.
306 5b. Although an over-simplification, this analysis highlights the variability of fault
307 zone components. Notably it shows that where the fault zone is very thick, Lower
308 Coralline fault products (lenses, breccia and cataclasite) occur on all outcrops of the
309 Maghlaq Fault (Fig. 5c), but in general only ever comprise up to 25% of the total fault
310 zone content, even though Lower Coralline Limestone comprises up to 50% of the
311 total faulted succession. As described later, only at major complexities in the fault
312 structure do Lower Coralline fault products contribute a significantly larger
313 proportion of the fault content.

314

315 *4.2. Globigerina Limestone*

316 Globigerina Limestone is preserved in the fault zone as intensely deformed
317 sheets that directly overly the Lower Coralline Limestone. Owing to its high porosity

and low inter-granular strength, the Globigerina Limestone has predominatly fragmented by the development of a network of deformation bands with associated localised granulation and grain comminution. This has resulted in fault breccias containing sub-rounded clasts up to 20cm long within a fine-grained matrix of granulated Globigerina Limestone (Fig. 9a).

Fault rock derived from the Globigerina Limestone is generally preserved in lensoid pods, restricted to the furrows of the corrugated footwall slip surface (Fig. 9b). Where measurable, the corrugations have strike-parallel lengths of 2 to >10m and amplitudes of 1 to 3m. We interpret the corrugations to result from the displacement of Lower Coralline Limestone lenses, which were incorporated within the fault zone by the coalescence of overlapping footwall slip surfaces or by shearing off of asperities from the footwall (Childs et al. 1996a,b; Ferrill et al. 1999). Outside of the corrugations, Globigerina Limestone fault rock is scarce, probably because it is friable material and was easily removed by the subsequent displacement of the Blue Clay and Upper Coralline Limestone down the fault. For this reason the Globigerina Limestone fault rocks are distributed erratically along the fault, as shown in Fig. 5c and Fig. 6.

4.3. Blue Clay

The Blue Clay Formation represents 40-86% of the exposed fault zone within the central part of the Maghlaq Fault trace between Ras Hanzir and Ras il-Hamrija (Fig. 5a; sections D-D', E-E', F-F' and G-G'). It reaches a maximum thickness of 22.5m at Ras Hanzir, where the basal contact of the Blue Clay with the underlying Globigerina Limestone can be seen within the fault zone (Fig. 5a; section D-D'). The Blue Clay is relatively undeformed in these areas, but green-blue depositional laminations in the sediment can be rotated approximately 30º towards the hangingwall

of the fault, as at Ras Hanzir and Ras il-Hamrija. Despite the large thickness of Blue Clay within the fault zone in the eastern exposures, the exposed thickness of Blue Clay along the western extent of the fault is <1m, such that no clay occurs within the fault zone at Ix-Xaqqa (Fig. 5a; section A-A'); although a data gap of 0.75m exists within this section, it occurs stratigraphically below the Blue Clay. In the absence of reverse movement within the fault zone, for which there is no evidence, the gap must represent eroded Globigerina Limestone. The extreme variability in clay thickness, represented schematically in Fig. 6, is best seen at Ras Hanzir (Fig. 5a). Here, the Blue Clay thickness varies from 0-22.5m over a 170m strike length of the fault (Fig. 5a; sections B-B', C-C' and D-D'). Relative to the *predicted* thickness, T_{LITH}, the Blue Clay is over-represented in the fault zone by a factor of 2-4 times, but where the fault zone is narrow the Blue Clay is absent.

4.4. Upper Coralline Limestone

The Upper Coralline Limestone sediments provide a continuous fault rock component along the length of the fault (Fig. 5c). They comprise a highly sheared belt, 2-10m wide, which is intensely foliated and separated from the less-deformed hangingwall by a discrete shear surface, or by a high strain zone (<0.5m wide) where the hangingwall beds are dragged and attenuated into parallelism with the fault (Fig. 6). Scarce remnants of the Greensand Formation outcrop sporadically as a discontinous layer along this contact, rotated parallel to the fault zone (Fig. 5a, section F-F').

5. Fault zone complexities

The Maghlaq Fault is a relatively simple structure over most of its length, comprising two principal slip surfaces that bound deformed rocks arranged in stratigraphic order from footwall to hangingwall. Areas of more complex geometry are located at branch-lines and at bends in the trace of the fault. These are interpreted to be sites of linkage of fault segments that were initially arranged in an en-echelon geometry. Below we present descriptions of a breached relay zone, branch-lines and mature fault bends which give rise to anomalous areas of complex fault zone structure along the Maghlaq Fault. Although similar complexities exist on normal faults of all sizes, their detailed characteristics are rarely described. The superb exposure afforded by the coastal outcrops along the length of the Maghlaq Fault, allow for both the analysis of fault zone structure and the interpretation of processes associated with its evolution.

5.1. Breached Relay Zone

At Tal-Gawwija (Fig. 4), part of a highly deformed rock volume between two overlapping fault segments of the Maghlaq Fault is exposed at the level of the basal contact of the Globigerina Limestone with the Lower Coralline Limestone (Fig. 10). The faults have a perpendicular separation of approximately 50m, between which the upper Lower Coralline Limestone contact defines a gently west-southwest dipping ramp. Although displacement variations on the hangingwall ramp-bounding fault cannot be demonstrated, the footwall fault displacement diminishes from about 30m, at the western edge of the relay ramp outcrop, to 7m approximately 180m to the ESE. These observations and the highly faulted nature of the ramp support our interpretation that the structure represents a highly deformed relay ramp, that is most

probably breached off-shore (Fig. 10a; Peacock and Sanderson 1994; Childs et al. 1995; Walsh et al. 1999).

The gross strike and dip of the relay ramp is broadly 170/07 WSW, defined by a best-fit surface of the Lower Coralline Limestone upper contact. Locally the Lower Coralline Limestone contact dips 15-45º SSW within decimetre-scale blocks bound by minor synthetic and antithetic faults within the relay ramp (Fig. 10b). The synthetic faults are common along the margins of the relay ramp and dip 53-89º SSW (average = 68º). In contrast, the antithetic faults dip 14-69º NNE (average = 39º) and are particularly well-developed within the centre of the relay ramp, where they comprise a hard-linked network (Fig. 10b). Synthetic faults accommodate near-pure dip-slip displacements (average lineation azimuth = 199º), whilst the antithetic faults consistently have a right-lateral slip component, on average trending 22.5º clockwise of the fault dip (average lineation azimuth = 043º). Antithetic faults account for approximately 70% of the extension accommodated in the ramp, and the maximum observed displacement of 5m is associated with an antithetic fault. A single cross-cutting relationship has been observed, where an antithetic fault with 5m displacement is offset 0.5m by a synthetic fault.

Synthetic ramp faults have similar dips to the ramp bounding faults and to synthetic faults outside the relay ramp. We suggest, therefore, that the synthetic faults have not rotated significantly as their dips are similar to the bulk shear plane of the fault zone. Poles to the synthetic and antithetic fault sets are asymmetrically distributed about the poles to bedding within the relay ramp (Fig. 10c). However, when layering within the rotated block is restored to horizontal and the antithetic faults are rotated by the same transformation, the two fault sets are broadly symmetrically distributed about the poles to bedding. This indicates that the antithetic

faults initiated as moderately dipping structures (average restored dip = 64º) and were subsequently passively rotated to shallower angles between the synthetic ramp faults. Oblique slip on the antithetic faults account for the fault parallel components of relay ramp dip.

In the proximity of the Tal-Gawwija relay ramp, bedding surfaces are present in the Lower Coralline Limestone, but have vertical spacings of 2-15m. Unlike relay ramps in strongly anisotropic multilayered rocks, where ramp rotation can be accommodated to a large extent by flexural slip along layering (Walsh et al. 1999), relay ramps in relatively massive successions must achieve a coherent deformation primarily through slip on different fault sets. The highly faulted nature of the relay ramp is consistent with data from other faults in Malta indicating that, relative to their displacements, fault frequencies (faults.m^{-1}) within breached relay ramps can be 1-2 orders of magnitude greater than elsewhere along the lengths of individual faults. The average common intersection orientation between the intra-relay faults (synthetic and antithetic), relay ramp bedding and ramp-bounding faults is 11/295 (Fig. 10c). This geometrical configuration provides a coherent means of ramp deformation by the intersection of opposed-dipping (synthetic/antithetic) fault sets within the plane of bedding-parallel slip surfaces. The precise details of the deformation are complex, but the overall WSW ramp dip is likely to result from a combination of fault-parallel rotations, which accommodate displacement transfer between fault segments, and local block rotations resulting from normal-oblique-dextral slip on the antithetic faults.

439 *5.2. Branch-lines*

440 Following the usage of Boyer and Elliot (1982), we refer to a branch-
441 line as the line of intersection between two segments of a multi-strand fault (see
442 Walsh et al. (1999) for 3-D examples associated with normal faults). The plunge and
443 azimuth of the branch-line depends on the relative orientations of the intersecting
444 faults and may range in attitude from horizontal to a maximum plunge equal to the dip
445 of the steeper fault. With fault exposures up to 40m high, the study area provides an
446 excellent opportunity to examine several steep to sub-vertical plunging branch-lines.
447 Here we describe the architecture of two examples.

448

449 5.2.1. Branch-line at Ras il-Hamrija

450 Between Halq it-Tafal and Denb il-Baghal, the Maghlaq Fault comprises two
451 principal fault traces, with a maximum separation of ca 100m (Fig. 4). At the Ras il-
452 Hamrija sea inlet, the 20m wide fault zone of the southernmost of the two principal
453 fault traces is intersected by a minor, east-northeasterly trending fault (throw = 9-
454 25m), which links to the northernmost principal fault trace (Figs 4 and 11a). The
455 minimum estimate of displacement on the northern and southern principal traces of
456 the Maghlaq Fault are approximately 37m and 105m, respectively. The linking fault is
457 tentatively interpreted as an abandoned relay-breaching fault (Peacock and Sanderson
458 1994; Childs et al. 1995; Walsh et al. 1999); the relay zone was finally breached along
459 a fault 120m to the east-southeast of the branch-line, now seen as a bend in the fault
460 trace (Fig. 11a).

461 The branch-line between the linking fault and the southern fault trace is well
462 exposed in 25m high cliffs, where the cliff surface is the footwall surface of the
463 southern principal fault (Figs 11a and 11b). The principal footwall fault surface has

been downthrown to the SE by the intersecting minor fault, giving a plan view offset of 4m (Fig. 11a, inset). By contrast the hangingwall slip surface of the fault zone is not offset, suggesting that it post-dates the formation of the branch-line, or the minor fault terminated within the major fault zone. The step in the footwall fault surface is filled with a moderately plunging (62/189) columnar wedge of coarsely brecciated Lower Coralline Limestone, with a subordinate volume of Globigerina Limestone breccia near the base (Fig. 11b). Near the top of the cliff, where erosion is subdued, a wedge of intensely brecciated footwall Lower Coralline Limestone, with a maximum horizontal length of about 8m, completely in-fills the step within the master fault surface. The breccia comprises angular clasts of Lower Coralline Limestone, 1mm-10cm long, which define a weak shape fabric dipping 55º-65º west at the accessible level of the outcrop. Although the breccia is cohesive, it maintains a fracture porosity of up to 5%.

In the proximity of the branch-line, two directions of fault slip occur on the southern principal fault surface. From over-printing relationships, the earlier features are metre-scale wavelength, low amplitude (ca 10cm) corrugations that pitch around 75º-80° ESE (Fig. 11c), oriented sub-parallel to the branch-line. These are post-dated by fine scratch and polish marks that plunge 65º-70° ESE. Although striations were not observed on the main intersecting fault, lineations on footwall splays to this fault indicate pure dip-slip to oblique WSW movement (Fig. 11c), accounting for the lateral offset of the principal fault across the branch-line. A minimum throw of 8.6m on the intersecting fault is necessary to obtain the observed 4m lateral offset of the principal fault, assuming a pure dip-slip displacement.

488 5.2.2. Branch-line at Halq it-Tafal

489 A complex branch-line is exposed in the footwall of the main Maghlaq Fault
490 surface in sea-cliff exposures, reaching nearly 30m high, at Halq it-Tafal (Figs 4 and
491 12a). The main east-southeast trending (118° strike) Maghlaq Fault is intersected at a
492 very acute angle (9°) by a footwall fault (109° strike) (Fig. 12a). Throws on the
493 footwall and hangingwall faults are 65-90m and >129m, respectively.

494 Unlike the previous example, the intersection line of the two fault planes
495 cannot be observed at Halq it-Tafal. Instead, the branch-line is marked by extensive
496 brecciation (minimum thickness = 5m), extending along strike of the fault zone for
497 90m (Fig. 12a and 12b). Poor outcrops preclude delineation of the complete extent of
498 the breccia into the footwall. However, given the intensity of the deformation, we
499 conjecture that brecciation occurs throughout a triangular wedge within the apex of
500 the intersecting faults. To the west, the breccia sheet pinches out to reveal a smooth
501 fault surface of the western fault plane (Fig. 12a). To the east, the breccia ends
502 abruptly, in a series of sheets that inter-finger with intensely fractured Lower
503 Coralline Limestone. As the branch-line is approached from the ESE, the dip of the
504 Lower Coralline Limestone increases from sub-horizontal to 24º WNW (Fig. 12b) and
505 is increasingly disrupted by synthetic and antithetic faults with centimetre to metre-
506 scale throws, illustrating the high strain at the branch-line.

507 Fault breccia associated with the branch-line is cohesive and contains angular
508 to moderately rounded clasts, with diameters of a few mm to several cm. Pore spaces
509 within the breccia are not occluded by cements, so that high porosities are preserved.
510 The breccia is overprinted by a weak fabric defined by minor slip surfaces and a
511 spaced fracture foliation oriented similarly to the footwall fault (Fig. 12c).
512 Additionally, a narrow east-southeasterly dipping fault zone cutting across the centre

513 of the wedge reworks and displaces the breccia by about 3m (Figs 12b and 12c),
514 accommodating localised slip sub-parallel to the branch-line.

515 Two slip directions are present in the vicinity of the Halq it-Tafal branchline
516 (Fig. 12c). One lineation is defined by subtle corrugations (wavelength=<1m;
517 amplitude=<0.1m) and polish marks that plunge steeply to the east (average =
518 61/201). A second slip direction is defined by gutter marks (Hancock and Barka,
519 1987), fine striations and polish marks that plunge less steeply towards the east
520 (average = 56/181). Cross-cutting relationships can be observed immediately west of
521 the breccia wedge, indicating that the shallower lineation is younger. This lineation
522 overprints the breccia wedge, indicating that it post-dates fault linkage (Fig. 12b).

523

524 5.2.3. Branch-line kinematics

525 Cross-cutting fault striations on the Maghlaq Fault have only been observed
526 within approximately 100m of the two major branch-lines, described above. We
527 suggest that the presence of two sets of striations indicates a change in the local fault
528 kinematics during the formation and subsequent modification of the branch-line. In
529 the Ras il-Hamrija example, the coincidence between the branch-line orientation and
530 that of the earliest preserved slip lineation on the principal fault (Fig. 11c) is
531 interpreted to indicate that the branch-line kinematically constrained the fault slip
532 direction, albeit transiently. Later fault striations that plunge more shallowly than the
533 branch-line probably reflect a return to the far-field slip direction, as the influence of
534 the branch-line became subdued by fault zone processes and/or by the abandonment
535 of the branch-line.

536 The occurrence of two slip orientations and their cross-cutting relationships in
537 the vicinity of the Halq it-Tafal branch-line (Fig. 12c) is remarkably similar to the Ras

538 il-Hamrija example (Fig. 11c) and also lends itself to an interpretation in which the
539 earlier lineation is kinematically controlled by the branch-line and the later lineation
540 reflects a return to the regional slip direction. The earliest slip lineation preserved
541 would, in this interpretation, reflect the average branch-line orientation between the
542 hangingwall fault (mean orientation=118/60 SSW) and the footwall fault, which
543 strikes 109º. The dip of the latter is unknown, but for our interpretation to be correct
544 could range between 56º and 62º, close to the modal fault dip value of 60º measured
545 along the Maghlaq Fault.

546 When faults of different orientation coalesce, the initial branch-line becomes
547 the axis of a bend on the modified normal fault surface (Fig. 13a). The range of
548 possible angular bend/branch-line orientations is a function of the relative attitudes of
549 the two intersecting faults (Figs. 13a, 13b and 13c) and may range from horizontal,
550 resulting from two parallel but unequally dipping faults, to steep, where the degree of
551 plunge is only limited by the dip of the steepest intersecting fault. In the case of faults
552 with relatively steep dips, the branch-line may plunge towards or away from the
553 direction of fault convergence (Figs. 13a and 13c). Given the large range of possible
554 branch-line orientations that could occur (Fig. 13c), the fact that the Ras il-Hamrija
555 and Halq it-Tafal examples are oriented sub-parallel to the approximately N-S (007º)
556 far-field slip direction of the Maghlaq Fault (Dart et al. 1993) suggests that they form
557 in relatively stable kinematic configurations. Other minor branch-lines at Ix-Xaqqa
558 (Fig. 4) are oriented parallel or sub-parallel to the far-field slip direction, as are fault
559 zone lens margins (Fig. 8) and fault surface corrugations (e.g. Il-Miqtub; Fig. 9).

560 The presence of a sharp bend on a fault surface at a branch-line represents a
561 physical obstacle to fault slip in directions other than parallel to the bend axis and, if
562 large enough, may cause fault slip to re-orient parallel to it, at least temporarily. Strain

563 compatibility problems (e.g. dilation and volume loss) about the angular bend at the
564 branch-line intersection would be minimal if the slip direction parallels the bend axis.
565 However, a bend oblique to the slip direction of the fault would represent either an
566 asperity to slip or a dilational bend. With increasing displacement, these are likely to
567 succumb to mechanical erosion, or would be in-filled by fault products, allowing the
568 fault slip direction to return to the far-field slip direction. Despite the small mismatch
569 between the branch-line orientations and the far-field slip direction at the two large
570 branch-lines described (5-10º), significant strain compatability problems occurred as
571 evidenced by the large breccia volumes generated adjacent to each.
572
573 *5.3. Fault Bends*
574 Distinct bends in the trace of the mainly ESE striking Maghlaq Fault are
575 defined by E-W striking portions, such as at Ras Hanzir and Ras il-Hamrija (Fig. 4),
576 which together define a left-stepping fault trace. The shorter, more E-W striking
577 portions are interpreted as footwall breaching faults arising from the growth and
578 failure of relay ramps between left-stepping fault segments (Childs et al. 1995; Ferrill
579 et al. 1999). Bends along the Maghlaq Fault are therefore interpreted as the examples
580 of long-established points of segment linkage. It follows that the fault bends represent
581 mature branch-lines.
582
583 5.3.1. Fault Bend at Ras Hanzir
584 At Ras Hanzir, the trace of the footwall slip surface changes in strike from
585 approximately 100º to 060º over 200m, defining a sharp footwall bend (Fig. 14a).
586 Between the apex of the bend and about 100m to the east, are a series of lens-shaped
587 lozenges of Lower Coralline Limestone (Fig. 14c). These range in scale from metres

588 to decametres: the larger lenses measure 30-50m parallel to the fault strike, up to 5m
589 thick and, prior to erosion, would have exceeded the vertical height of the cliff
590 exposures (>35m)(Fig. 14c). These E-W striking lenses overlap in a left-stepping
591 sense about the western part of the bend (Fig. 14a). The apparent flat-topped nature of
592 the lenses is interpreted as the contact of the Lower Coralline Limestone with the less
593 resistant (now eroded) Globigerina Limestone. A decrease in the elevation of these
594 flat tops towards the apex of the bend (i.e. southwesterly) therefore reflects an
595 increase in the displacement of the lenses. A lens of highly deformed Globigerina
596 Limestone on the bend apex represents the furthest travelled lens (Fig. 14a and 14c).
597 The fault trace defined by the hangingwall of the lenses is more smoothly curved than
598 that of the footwall (Fig. 14a), indicating that the angularity of the fault has been
599 decreased by the mechanical erosion of the footwall limestones into lenses and by
600 their subsequent internal deformation and translation in the fault zone. The poles to
601 the curved footwall fault surface at Ras Hanzir plot as a great circle on a stereonet,
602 oriented 090/19N (Fig. 14c), indicating that the fault bend approximates a
603 cylindrically curved surface (Fig. 14b). A near-constant slip azimuth about the bend
604 of 70/180 is achieved by a systematic change in the lineation pitch, from 71ºE in the
605 west, to 67ºW in the east. This slip direction is very similar to the 007º far-field
606 extension direction determined by Dart et al. (1993). The development of the
607 cylindrical fault bend axis in the orientation of the regional slip direction maintains
608 strain compatibility while reducing surface area, hence frictional resistance to fault
609 slip.
610

611 5.3.2. Fault Bend at Ras il-Hamrija

612 A similar, but less accessible, example of a fault bend outcrops in the sea cliffs
613 approximately 100m east of Ras il-Hamrija (Fig. 4 and 11a). Here the main trace of
614 the Maghlaq Fault changes in strike from approximately 130º to 80º. A decametre-
615 scale scoop-shaped lens, derived from the footwall Lower Coralline Limestone and
616 Globigerina Limestones, occupies the apex of the bend (Fig. 15). The lens is
617 approximately 65m wide, 20m thick and >35m high and has been displaced vertically
618 8-10m along the footwall slip surface. The lens appears to have undergone some
619 rotation in sympathy with the fault displacement, indicated by the 30-40ºS dip of the
620 Lower Coralline contact with the Globigerina Limestone, revealed by partial erosion
621 of the less resistant, younger limestone. However, deformation of the lens appears less
622 intense than at Ras Hanzir, with only one other lens being partially exposed lower
623 down in the cliff face (Fig. 15).

624

625 **6. Discussion**

626 This discussion considers three main questions. What were the fundamental
627 controls on the development of the structure and content of the Maghlaq Fault Zone
628 during its growth? How does the Maghlaq Fault Zone differ from other faults and
629 what factors are responsible for these differences? Finally, how might the
630 heterogeneous nature of the structure and content of fault zones, as observed in the
631 Maghlaq Fault, influence fluid flow in similar fault systems?

632

633 *6.1. Development of the Maghlaq Fault Zone*

634 The absence of faults of similar orientation and size close to the Maghlaq Fault
635 suggest that its individual segments formed as elements of a coherent fault array

636 (Walsh et al. 2003). The systematic arrangement of the segments as a left-stepping
637 array suggests an underlying basement control on their locations. We suggest that the
638 Maghlaq Fault formed by upward propagation during early extension, associated with
639 the development of the Pantelleria Rift during Burdigalian times (Dart et al. 1993).

640 The breached relay, branch-lines and bends documented here illustrate
641 progressive stages of linkage between the individual strands of a segmented normal
642 fault (e.g. Peacock and Sanderson 1991, 1994; Childs et al. 1995, 1996a; Ferrill et al.
643 1999; Walsh et al. 1999, 2003) and most of the structural complexities of the Maghlaq
644 Fault can be explained in these terms. Elevated strains occur within relay zones to
645 accommodate ramp rotation (e.g. the relay ramp at Tal-Gawwija). Eventually strain
646 within the relay zone can no longer be accommodated by ramp deformation and the
647 relay zone becomes breached by linkage between the two bounding faults to form a
648 through going fault (Peacock and Sanderson 1991; Childs et al;. 1995). The site of
649 the former relay zone is preserved as a bend or dog-leg on the trace of the new
650 continuous fault (e.g. Ras Hanzir and Ras il-Hamrija). The axis of the bend in the
651 fault surface is unlikely to be oriented exactly parallel to the overall fault slip vector
652 and the bend will therefore remain a focus for high strain. This fault surface
653 irregularity can be removed by minor modification of the active slip surface, as for
654 example the footwall of the fault bend at Ras Hanzir, or by creation of a new linking
655 fault to form a fault bounded lens, as in the case of Ras il-Hamrija.

656 Progressive breaching of relay ramps, straightening of fault bends and removal
657 of fault irregularities gives rise to complex and anomalously wide fault zones. These
658 processes reduce the overall active trace length of the fault and smooth fault surfaces.
659 These modifications both reduce the frictional resistance to slip on the fault surface

660 and the requirement for volumetric strains associated with fault sidewall
661 incompatibility.

662 There are no intact relay ramps along the exposed trace of the Maghlaq Fault
663 but fault bends representing the sites of large scale relay zones (100m separation) are
664 still apparent. There is however an absence of distinct fault segments spaced <50m.
665 While it might be possible that segmentation did not occur on the smaller scale, we
666 consider it far more likely that segment boundaries with low separations were
667 consumed into the fault zone at displacements significantly lower than that at the
668 present day. The many lenses that occur within the fault zone (e.g. Fig. 8) represent
669 possible sites of former segment boundaries on all scales below 50m. There are few
670 means of establishing whether a lens within a fault zone formed by breaching of a
671 segment boundary or by the shearing off of an asperity on an already through-going
672 fault. In certain circumstances it may be possible to differentiate on the basis of
673 structural position, e.g. the lenses on the fault bend at Ras Hanzir probably formed by
674 modification of the footwall of a through going fault. In most cases the distinction
675 between these two alternatives will be vague in that much fault surface irregularity
676 will be inherited from the initial segmented character of the fault. Once a lens has
677 been incorporated within a fault zone, it may be dissected into smaller lenses by the
678 formation of Riedel shears (Fig. 8b) and the lens margins, effectively branchlines
679 between slip surfaces, become sites of intense brecciation (Fig. 8c).

680 We contend that the major structures within the footwall Lower Coralline
681 Limestone exposures developed during the initial 100-160m of displacement, prior to
682 the juxtaposition of the unlithified hangingwall sediments. The range in these
683 displacements reflects the height of the outcropping fault exposures with respect to
684 the level of the Blue Clay in the hangingwall. We suggest that once the Lower

685 Coralline Limestone was juxtaposed against the Blue Clay and Upper Coralline
686 Limestone, it was energetically preferable for asperities to be accommodated by
687 continuous deformation of the low yield strength hangingwall sediments rather than
688 by the creation of new fractures in the lithified footwall. Therefore, at this time, the
689 footwall deformation would have effectively ceased following segment linkage and
690 lens formation at locations such as the Ras Hanzir bend. Following linkage of the
691 segments, the Blue Clay and Upper Coralline Limestone Formations deformed by
692 macroscopic ductile flow, attenuating into sheets of fault rock.
693
694 *6.2. Comparison to other fault zones*
695 Some previous studies of faulted carbonate rocks have highlighted the crucial
696 role of pressure solution processes in all aspects of faulting, e.g. fault nucleation
697 (Willemse et al. 1997; Peacock et al. 1998; Graham et al. 2003), the accommodation
698 of volumetric strains (Odonne and Massonat, 1992), especially displacement gradients
699 around fault tips (Petit and Mattauer, 1995), and the removal of asperities to fault slip
700 (Gratier and Gamond, 1990; Childs et al. 1996a). The absence of features associated
701 with significant pressure solution processes in the Maghlaq Fault Zone, at the exposed
702 level, is attributed to the very shallow burial depths at the time of faulting, although
703 we consider it highly likely that these processes played an important role at deeper
704 levels. The lack of pressure solution and the relatively massive nature of the
705 Globigerina Limestone and Lower Coralline Limestone, which diminishes the
706 likelihood of flexural slip, restricts the manner in which strain can be accommodated
707 and favours deformation by small-scale fracture processes. Possible manifestations of
708 this are the extensive deformation band arrays in more highly strained areas of the
709 footwall and the development of Riedel shears (Fig. 8c) and microfractures within

710 fault lenses. Furthermore, the paucity of vein material and fault rock cements in the
711 Maghlaq Fault Zone, contrasts with other faults in limestone where pressure solution
712 processes have been demonstrated to be the predominant source of the vein material
713 (Gratier et al. 1993) and accounts for the highly porous appearance of breccias within
714 branch-lines.
715
716 *6.3. Implications for fault-related fluid flow*
717 With the exception of the Blue Clay Formation, the faulted strata contain
718 intervals of moderate to highly porous rock. Therefore, neglecting the content of the
719 fault zone, the relative juxtaposition of lithologies other than the Blue Clay would, in
720 general, favour across-fault fluid flow. Only where the Blue Clay is present would the
721 arrangement of wall rocks provide a juxtaposition seal that might retard or prevent
722 across-fault flow (Nybakken, 1991). The Blue Clay is, however, a significant
723 component of the fault zone and its presence along the majority of the exposed fault
724 trace suggests that it forms an extensive and continuous fault rock layer. In sub-
725 surface fluid flow systems the presence of the Blue Clay would be expected to retard
726 flow, either by forming a low permeability barrier to across-fault fluid flow or, in the
727 case of hydrocarbon flow, by defining an impermeable membrane to across-fault flow
728 (due to the typically high entry pressures of clays; Nybakken, 1991; Manzocchi et al.
729 1992). However in the western end of the fault trace, Ix-Xaqqa and central Ras
730 Hanzir, Blue Clay fault rock is absent. At these localities the fault displacement is
731 about 4 times the clay bed thickness. Clay fault rock continuity data collected from
732 siliciclastic sequences suggests, however, that clay smears are often continuous for
733 displacement:source layer thickness ratios of ~7 or less (Lindsay et al. 1993; Yielding
734 2002). The reason for the local absence of Blue Clay at relatively low

735 displacement:thickness ratios (~7) is not understood, but it may arise from local
736 geometrical effects of the fault or from issues relating to the rheological properties of
737 the faulted sequence or the deformation conditions associated with faulting.

738 At depths below the level of the Blue Clay in the hangingwall, the content of
739 the fault zone must comprise fault products derived from the Lower Coralline
740 Limestone, with or without Globigerina Limestone. The Globigerina Limestone is
741 highly porous and the Lower Coralline Limestone contains porous intervals, therefore
742 a juxtaposition seal over a significant vertical extent is unlikely. However, fine-
743 grained cataclasites that coat the polished principal slip surfaces within the Lower
744 Coralline Limestone-derived fault products (Figs 7b and c) have extremely low
745 porosities and, we presume, low permeabilities. Their low permeability combined
746 with their relatively continuous distribution over the fault surface provides some
747 potential for a decrease in across-fault flow.

748 The presence of internally fractured lensoid volumes of Lower Coralline
749 Limestone and Globigerina Limestone within the fault zone suggests potential for
750 along-fault fluid flow particularly around the fractured and brecciated fringes of
751 lenses. Our limited data from the Maghlaq Fault and elsewhere in Malta suggests that
752 the lenses tend to have long axes parallel to their dip direction, with their intersections
753 parallel to the slip direction, imparting a strong up-fault fracture anisotropy.

754 The potentially most significant areas for fluid flow within the fault zone are
755 the sites of fault segment linkage (breached relays, branch-lines and bends) which
756 correspond to areas with the largest thicknesses of fractured rock. In 3-dimensions,
757 the linkage structures can extend vertically to a branch-point, or sub-horizontal
758 branch-line where the fault tip-line originally bifurcates (Childs et al. 1995; Huggins
759 et al. 1995; Ferrill et al. 1999; Walsh et al. 1999). It follows that they can represent 1-

760 dimensional conduits of considerable vertical extent, oriented broadly parallel to the
761 fault slip direction. These structures therefore have great potential for tapping deep-
762 seated fluid reservoirs. Indeed, localised up-fault flow of hydrothermal ore fluids
763 within breached relay zones and branch-lines is recognised as an important control on
764 the location of carbonate-hosted Zn-Pb(-Ba) deposits in the Irish orefield (Carboni et
765 al. 2003) and are likely to be important elsewhere. Similarly, in hydrocarbon systems,
766 these structures may represent migration fairways, as shown by Garden et al. (2001),
767 but may also correspond to potential leakage points. Recognition of the depth at
768 which the fault initially bifurcates is critical in the assessment of the potential for up-
769 fault fluid flow. In general, the greater the separation of the original fault segments
770 linked by the relay, branch-line or bend, the deeper the tip-line bifurcation point
771 extends.
772
773 **7. Conclusions**
774 1. The Maghlaq Fault formed within a carbonate succession at shallow burial
775 depths (<250m). The rocks are not affected by pressure solution and maintain
776 significant fault rock porosity.
777 2. The large-scale structure of the Maghlaq Fault Zone is interpreted to have
778 evolved through linkage of an initially left-stepping, segmented normal fault. Fault
779 zone heterogeneities demonstrate stages in the breaching of relay zones at fault
780 segment boundaries with increasing displacement.
781 3. The fault zone comprises lenses of variably deformed rock bound by discrete
782 slip surfaces over a broad range of scales. The lensoid geometry is due to the
783 breaching of relay zones and fault segment linkage, the inclusion of asperities and the
784 development of minor slip surfaces within the fault zone (e.g. Riedel shears).

4. Fault rock distribution varies from Lower Coralline Limestone derived cataclasites, found over the whole fault surface, to localised breccia pods derived from Globigerina Limestone, reflecting differences in the degree of lithification of the wall rock units at the time of faulting.

5. The fault rocks, derived from fully lithified sediments at the time of faulting, comprise fine-grained veneers of cataclasite and coarse poorly cemented breccias. Breccia development is largely associated with branchlines between connecting faults in response to volumetric strains due to non-colinearity of fault branch-lines and slip vectors.

6. Deformation of the Lower Coralline Limestone in the footwall to the fault zone is restricted to locally developed arrays of cataclastic deformation bands. These arrays may reach several metres in width where fault segments overlap.

7. Fault rock distribution suggests that in general the Maghlaq Fault will provide a barrier to across fault flow, but a conduit to fault parallel flow. Up-fault flow is especially likely at areas of fault heterogeneity.

Acknowledgements

The authors gratefully acknowledge ENI Exploration and Production Division (Milan) for funding this research and Janpieter van Dijk for supporting the project throughout. We are indebted to Chris Dart for advice on potential field localities in Malta and the loan of his thesis, and to Martyn Pedley for valuable information on Maltese geology. Finally we thank Davis Peacock and Nigel Woodcock for their reviews.

809 **References**

810 Aydin, A., Johnson, A.M., 1978. Development of faults as zones of deformation
811 bands and as slip surfaces in sandstone. Pure and Applied Geophysics **116**, 931-
812 942.

813 Bennett, S.M., 1980. Palaeoenvironmental studies in Maltese mid-Tertiary carbonates.
814 Unpublished PhD thesis, University of London.

815 Bosence, D.W.J., Pedley; H.M., 1982. Sedimentology and palaeoecology of a
816 Miocene coralline algal bioherm from the Maltese islands. Palaeogeography,
817 Palaeoclimatology and Palaeoecology **38**, 9-43.

818 Boyer, S.E., Elliot, D., 1982. Thrust systems. American Association of Petroleum
819 Geologists Bulletin **66**, 1196-1230.

820 Cello, G., Crisci, G.M., Marabini, S., Tortorici, L., 1985. Transtensive tectonics in the
821 Strait of Sicily: structural and volcanological evidence from the island of
822 Pantelleria. Tectonics **4**, 311-322.

823 Childs, C., Watterson, J., Walsh, J. J. 1995. Fault overlap zones within developing
824 normal fault systems. Journal of the Geological Society, London **152**, 535-549.

825 Childs, C., Nicol, A., Walsh, J.J., Watterson, J. 1996a. Growth of vertically
826 segmented normal faults. Journal of Structural Geology **18**, 1389-1397.

827 Childs, C., Watterson, J., Walsh, J.J. 1996b. A model for the structure and
828 development of fault zones. Journal of the Geological Society, London **153**, 337-
829 340.

830 Dart, C.J., 1991. Carbonate sedimentation and extensional tectonics in the Maltese
831 graben system. Unpublished PhD thesis, University of London.

832 Dart, C.J., Bosence, D.W.J., McClay, K.R. 1993. Stratigraphy and structure of the
833 Maltese Islands. Journal of the Geological Society, London **150**, 1153-1166.

834 Finetti, I. 1982. Structure, stratigraphy and evolution of the central Mediterranean.
835 Bollettino di Geofisica Teorica ed Applicata **24**, 247-312.
836 Ferrill, D.A., Stamtakos, J.A., Sims, D. 1999. Normal fault corrugation: implications
837 for growth and seismicity of active normal faults. Journal of Structural Geology **21**,
838 1027-1038.
839 Foxford, K.A., Walsh, J.J., Watterson, J., Garden, I.R., Guscott, S.C., Burley, S.D.
840 1998. Structure and content of the Moab Fault Zone, Utah, U.S.A., and its
841 implications for fault seal prediction. In: Jones, G., Fisher, Q.J. and Knipe, R.J.
842 (Eds), Faulting, Fault Sealing and Fluid Flow in Hydrocarbon Reservoirs.
843 Geological Society of London, Special Publication **147**, 87-103.
844 Garden, I.R., Guscott, S.C., Burley, S.D., Foxford, K.A., Walsh, J.J., Marshall, J.
845 2001. An exhumed palaeo-hydrocarbon migration fairway in a faulted carrier
846 system, Entrada Sandstone of SE Utah, USA. Geofluids **1**, 195-213.
847 Gawthorpe, R.L., Sharp, I., Underhill, J.R., Gupta, S. 1997. Linked sequence
848 stratigraphic and structural evolution of propagating normal faults. Geology **25**,
849 795-798.
850 Graham, B., Antonellini, M., Aydin, A. 2003. Formation and growth of normal faults
851 in carbonates within a compressive environment. Geology **31**, 11-14.
852 Gratier, J.P., Gamond, J.F. 1990. Transition between seismic and aseismic
853 deformation in the upper crust. In: Knipe, R.J., Rutter, E.H. (Eds), Deformation
854 mechanisms, rheology and tectonics. Geological Society, London, Special
855 Publication **54**, 461-473.
856 Gratier, J.P., Chen, T., Hellmann, R. 1994. Pressure solution as a mechanism for crack
857 sealing around faults. In: Hickman, S.H., Sibson, R.H., Bruhn, R.L. (Eds),

858 Mechanical involvement of fluids in faulting. USGS Open File Report **228**, 279-
859 300.
860 Hancock, P.L., Barka, A.A. 1987. Kinematic indicators on active normal faults in
861 western Turkey. Journal of Structural Geology **9**, 573-584.
862 Hill, K.C., Hayward, A.B. 1988. Structural constraints on the Tertiary plate tectonic
863 evolution of Italy. Marine and Petroleum Geology **5**, 2-16.
864 Huggins, P., Watterson, J., Walsh, J. J., Childs, C. 1995. Relay zone geometry and
865 displacement transfer between normal faults recorded in coal mine plans. Journal
866 of Structural Geology **17**, 1741-1755.
867 Jongsma, D., vanHinte, J.E., Woodside, J.M. 1985. Geological structure and
868 neotectonics of the north African continental margin south of Sicily. Marine and
869 Petroleum Geology **2**, 156-177.
870 Lindsay, N. G., Murphy, F. C., Walsh, J. J., Watterson, J. 1993. Outcrop studies of
871 shale smears on fault surfaces. In: Flint, S., Bryant, I. D. (Eds), The geological
872 modelling of hydrocarbon reservoirs and outcrop analogues. Special Publication of
873 the International Association of Sedimentologists **15**, 113-123.
874 Maltman, A. 1994. Deformation structures preserved in rocks. In: Maltman, A. (ed.),
875 The geological deformation of sediments. Chapman and Hall, London, 261-302.
876 Manzocchi, T., Heath, A.E., Walsh, J.J. & Childs, C. 2002. The representation of two
877 phase fault-rock properties in flow simulation models. Petroleum Geoscience **8**,
878 119-132.
879 Nybakken, S. 1991. Sealing fault traps – an exploration concept in a mature petroleum
880 province: Tampen Spur, northern North Sea. First Break **9,** 209-222.

881 Odonne, F., Massonnat, G. 1992. Volume loss and deformation around conjugate
882 fractures: comparison between a natural example and analogue experiments.
883 Journal of Structural Geology **14**, 963-972.
884 Peacock, D.C.P., Sanderson, D.J. 1991. Displacements and evolution of fault
885 segments: example of an extensional fault system at Kilve, Somerset. Journal of
886 Structural Geology **13**, 721-733
887 Peacock, D.C.P. & Sanderson, D.J. 1994. Geometry and development of relay ramps
888 in normal fault systems. Bulletin of the American Association of Petroleum
889 Geologists **78**, 147-165.
890 Peacock, D.C.P., Fisher, Q.J., Willemse, E.J.M., Aydin, A., 1998. The relationship
891 between faults and pressure solution seams in carbonate rocks and the implications
892 for fluid flow. In: Jones, G., Fisher, Q.J., Knipe, R.J. (Eds), Faulting, fault sealing
893 and fluid flow in hydrocarbon reservoirs. Geological Society, London, Special
894 Publication **147**, 105-115.
895 Pedley, H.M. 1978. A new lithostratigraphical and palaeoenvironmental interpretation
896 for the coralline limestone formations (Miocene) of the Maltese Islands. Overseas
897 Geology and Mineral Resources, H.M.S.O. London, **54**, pp. 17.
898 Pedley, H.M. 1987a. Controls on Cenozoic carbonate deposition in the Maltese
899 Islands: review and interpretation. Memorie della Società Geologica Italiana **38**,
900 81-94.
901 Pedley, H.M. 1987b. The Ghar Lapsi limestones: sedimentology of a Miocene intra-
902 shelf graben. Centro **1**, 1-14.
903 Pedley, H.M. 1990. Syndepositional tectonics affecting Cenozoic and Mesozoic
904 deposition in the Malta and SE Sicily areas (Central Mediterranean) and their

905 bearing on Mesozoic reservoir development in N Malta offshore region. Marine
906 and Petroleum Geology **7**, 171-180.
907 Pedley, H.M. 1993. Geological map of the Islands of Malta, 1:25,000 scale. British
908 Geological Survey, Keyworth, Nottinghamshire, UK.
909 Pedley, H.M. 1996. Miocene reef facies of the Pelagian region (central
910 Mediterranean). Models for Carbonate Stratigraphy from Miocene Reef
911 Complexes of the Mediterranean Regions. SEPM Concepts in Sedimentology and
912 Palaeontology **5**, 247-259.
913 Pedley, H.M. 1998. A review of sediment distributions and processes in Oligo-
914 Miocene ramps of S. Italy and Malta (Mediterranean divide). In: Wright, V.P. and
915 Burchette, T.P. (Eds), Carbonate Ramps. Geological Society, London, Special
916 Publication **149**, 163-179.
917 Pedley, H.M., Bennett, S.M. 1985. Phosphorites, hardgrounds and syndepositional
918 solution subsidence: a paleoenvironmental model from the Miocene of the Maltese
919 Islands. Sedimentary Geology **45**, 1-34.
920 Pedley, H.M., House, M.R., Waugh, B., 1976. The geology of Malta and Gozo.
921 Proceedings of the Geological Association **87**, 325-341.
922 Petit, J.P., Mattauer, M. 1995. Palaeostress superimposition deduced from mesoscale
923 structures in limestone; the Matelles exposure, Languedoc, France. Journal of
924 Structural Geology **17**, 245-256.
925 Reuther, C.-D., Eisbacher, G.H., 1985. Pantelleria Rift: crustal extension in a
926 convergent intraplate setting. Geologische Rundschau **74**, 585-597.
927 Sibson, R.H. 1977. Fault rocks and fault mechanisms. Journal of the Geological
928 Society, London **133**, 191-213.

929 Walsh, J.J., Watterson, J., Bailey, W.R., Childs, C. 1999. Fault relays, bends and
930 branchlines. Journal of Structural Geology **20**, 1019-1026.
931 Walsh, J.J., Bailey, W.R., Childs, C., Nicol, A., Bonson, C.G., 2003. Formation of
932 segmented normal faults: a 3-D perspective. Journal of Structural Geology **25**,
933 1251-1262.
934 Willemse, E.J.M., Peacock, D.C.P., Aydin, A., 1997. Nucleation and growth of strike-
935 slip faults in limestone. Journal of Structural Geology **19**, 1461-1477.
936 Yielding, G. 2002. Shale gouge ratio – calibration by geohistory. In: Koestler, A.G.
937 and Hunsdale, R. (Eds) Hydrocarbon Seal Quantification. Norwegian Petroleum
938 Society (NPF), Special Publication **11**, 1-15.
939
940
941 **Figure captions**
942
943 Fig. 1. Map of the central Mediterranean region showing the location of the Maltese
944 archipelago with respect to the Pantelleria Trough and Maghrebian-Apennine thrust
945 and fold belt (after Dart et al. 1993).
946
947 Fig. 2. Map showing the locations of major normal faults in the Maltese islands
948 together with an interpretation of 2-D seismic lines from the northern part of the
949 Pantelleria Rift, both from Dart et al. (1993). The Maghlaq Fault is located on the SW
950 coast of Malta and represents the most northerly extent of the Pantelleria Rift fault
951 trend. Horizon contoured for two-way time (seconds; 1sec ≈ 1km).
952

953 Fig. 3. Tectono-stratigraphic log of the Oligocene-Quaternary age sediments of the
954 Maltese archipelago (modified from Dart et al. 1993). Stratigraphic thickness ranges
955 are given for onshore Malta and values in parentheses are local thicknesses, measured
956 by Pedley (1993) from the mapped geology in the footwall of the Maghlaq Fault. EP.
957 denotes 'Epoch', with P-H representing Pleistocene to Holocene age, which is
958 otherwise referred to as Quaternary in the text.
959
960 Fig. 4. Geological map of the Maghlaq Fault study area. Individual members of the
961 stratigraphic formations are not distinguished on the map. Topographic contour
962 intervals are in metres. Grid references are in UTM coordinates (datum: WGS84,
963 projection: NUTM33).
964
965 Fig. 5. (a) Simplified map of the Maghlaq Fault Zone indicating positions of fault
966 zone sections A-A' to I-I'. The fault zone, defined by well-defined shear boundaries,
967 is indicated beneath each section by a bar. (b) Schematic diagram illustrating
968 parameters used to calculate *predicted* fault zone lithology thickness, T_{LITH}. (c) Plot of
969 true thickness/predicted thickness for each fault zone lithology vs total fault zone
970 thickness measured in the field. Section C-C' is not represented due to uncertainty
971 regarding the maximum fault zone thickness at this locality.
972
973 Fig. 6. Schematic 3-D diagram illustrating the main characteristics of the internal
974 structure of the Maghlaq Fault Zone at the current exposure level. The principal
975 features illustrated are as follows: (i) Footwall Lower Coralline Limestone is
976 relatively undeformed outside the fault zone, apart from areas close to the fault that
977 are sporadically affected by arrays of deformation bands, particularly near fault

978 irregularities. (ii) Lenses of footwall Lower Coralline Limestone are incorporated into
979 the fault zone. The lenses typically show internal deformation by Riedel shears and
980 they are intensely brecciated where they thin towards their margins. (iii) Overlapping
981 lenses of footwall-derived limestone are derived by the mechanical attrition of an
982 angular bend (formerly a branch-line). (iv) Highly brecciated footwall limestone
983 defines a branch-line between major fault segments. (v) Highly discontinuous lenses
984 of deformed Globigerina Limestone. (vi) Blue Clay fault zone component is
985 characterised by rapid thickness changes but relatively high continuity within the fault
986 zone. (vii) Highly continuous hangingwall shear zone comprising deformed Upper
987 Coralline Limestone. (viii) Moderately dipping hangingwall Upper Coralline
988 Limestones contain slumps and minor antithetic faults. It should be noted that the
989 fault slip direction is slightly oblique to the dip direction, as indicated by the small
990 disparity in the arrows (slip direction) and the dashed lines (dip direction) on the fault
991 surface. Although an approximate scale is presented, the structures shown can occur
992 over a range of scales within an individual fault system.
993
994 Fig. 7. Faulted Lower Coralline Limestone. (a) Fault-related deformation bands in the
995 footwall at Ras il-Hamrija (see Fig. 4 for location). The shears are more resistant than
996 the host Lower Coralline Limestone and therefore weather as prominent ridges. (b)
997 Prominent Lower Coralline Limestone fault surfaces of the Maghalq Fault which
998 constitute resilient sea cliffs between Tal-Gawwija and Ras il-Hamrija (see Fig. 4).
999 Cliff height is 30-40m. (c) Photomicrograph of the sharp boundary between fine
1000 grained, cataclastically deformed Lower Coralline Limestone fault rock and the
1001 relatively undeformed protolith. (d) Highly porous Lower Coralline Limestone
1002 breccia comprising coarse angular fragments. The compass-clinometer is 10cm long.

1003

1004 Fig. 8. Lower Coralline Limestone lenses within the Maghlaq Fault Zone. (a) Photo-
1005 montage of lens formed by coalescence of overlapping slip surfaces at Ix-Xaqqa. The
1006 lens is elongate down dip and is bound by steeply plunging branch-lines, of similar
1007 orientation to the slip striations. The height of the outcrop is approximately 25m. (b)
1008 Oblique view of a lens margin at Ras Hanzir. Riedel shears cut through the lens
1009 causing thinning and elongation. Lens thickness is approximately 60cm. (c) Tapering
1010 basal and lateral fringes of a lens at Ras Hanzir (lens 7 on Fig. 14a and 14b). Both
1011 margins comprise cohesive fault breccia, but the lens core is relatively intact. Note the
1012 similarity in orientation of the lateral margins of the lens with the fault striations.

1013

1014 Fig. 9. Faulted Globigerina Limestone. (a) Highly disaggregated Globigerina
1015 Limestone breccia juxtaposed against polished Lower Coralline Limestone slip
1016 surface at Ras Hanzir (Fig. 4). Approaching the slip surface the fault rock grades from
1017 a jigsaw breccia (top-right) to a coarse breccia of sub-rounded cm-scale clasts in a
1018 moderately cohesive fine-grained matrix. The notebook is 20cm long. (b) Map of the
1019 fault zone exposed in the Il-Miqtub sea inlet (Fig. 4), illustrating the occurrence of the
1020 Globigerina Limestone within the fault zone as discontinuous lenses, commonly
1021 restricted to concave corrugations on the footwall slip surface.

1022

1023 Fig. 10. (a) Interpreted aerial photograph of the Tal-Gawwija breached relay ramp.
1024 The boxed area denotes the position of Fig. 10b. The trace of the inferred breaching
1025 fault offshore is unknown. (b) Baseline grid map of the breached relay (boxed area in
1026 Fig. 10a). Relay deformation is accommodated by a network of synthetic and
1027 antithetic faults that cause locally high bed dips. Towards the S of the exposure,

1028 solution erosion is intense and the relay deformation is mapped in less detail. (Cairn is
1029 located at E0449713 N3964397). (c) Equal area stereonet of structural data from the
1030 relay ramp. The pole to the fitted great circle represents the common intersection
1031 point of intra-relay faults (synthetic and antithetic), relay bedding and ramp-bounding
1032 faults.
1033
1034 Fig. 11. (a) Geological map of the studied Ras il-Hamrija branch-line. Point 'p'
1035 denotes the position of the viewpoint for Fig. 11b, whilst Point 'q' shows the
1036 viewpoint for Fig. 15. The hangingwall structure is supplemented with data from Dart
1037 (1991). Inset: sketch map enlargement of the offset trace of the principal fault. (b)
1038 Photo-montage of the branch-line intersection with the polished main footwall slip
1039 surface of the Maghlaq Fault, exposed as southwesterly facing cliff, viewed towards
1040 the ESE. The fault intersection is marked by a steeply inclined zone of coarsely
1041 brecciated Lower Coralline Limestone (highlighted by arrows) and, at the base of the
1042 outcrop, Globigerina Limestone breccia. (c) Equal area stereonet of fault data derived
1043 from the branch-line area. Note the close coincidence between fault slip lineations on
1044 the 'master' fault and the branch-line orientation.
1045
1046 Fig. 12. (a) Geological map of the branch-line outcropping at Halq it-Tafal. Point 'p'
1047 denotes the viewpoint of Fig. 12b. (b) View looking ESE along the brecciated Lower
1048 Coralline Limestone at the apex of the branch-line. Immediately beyond the breccia,
1049 the contact of the Lower Coralline Limestone with the Globigerina Limestone is
1050 dragged towards the branch-line apex. In the distance the Lower Coralline Limestone
1051 beds are flat-lying. The cliff height in the foreground is approximately 30m. (c) Equal
1052 area stereonet of fault data derived from the branch-line area.

1053

1054 Fig. 13. (a) Schematic diagrams illustrating the variability in branch-line orientations
1055 between a 60º dipping principal fault and an intersecting fault with dips of 60º, 40º
1056 and 80º. Black arrows represent the far-field extension direction. Dashed grey arrows
1057 represent branch-line parallel slip, i.e. slip which minimizes related strain
1058 compatibility problems. (b) Scheme of measurements used on plot Fig. 13c. (c) Plot
1059 showing the variation in branch-line pitch on a 60º dipping principal fault for varying
1060 angles of intersection of footwall intersecting faults that range in dip from 1º to 89º
1061 (labelled curves). For intersecting faults steeper than the principal fault, the angle of
1062 intersection may plunge in the direction of fault trace convergence. Intersecting faults
1063 dipping less than the principal fault always plunge away from the direction of fault
1064 trace convergence.

1065

1066 Fig. 14. (a) Geological map of the Ras Hanzir fault bend, illustrating the rapid
1067 changes in fault zone thickness from west to east and the development of a series of
1068 stacked lenses, annotated 1 to 7. (Point ‘p’ denotes the position of the viewpoint of
1069 Fig. 14c). (b) Stereonet of fault data derived from the footwall slip surface of the fault
1070 bend. (c) View of the overlapping lenses on the footwall slip surface, looking WNW.
1071 Fault zone lenses are annotated 1 to 7 in relation to Fig. 14a. Note the person for scale
1072 (circled).

1073

1074 Fig. 15. Photograph of a large scoop-shaped lens on the bend apex at Ras il-Hamrija,
1075 looking WNW (viewpoint is shown in Fig. 11a; point ‘q’). The lens measures about
1076 65m wide, 20m thick and >35m high, and has been displaced vertically 8-10m along
1077 the footwall slip surface. Cliff height is approximately 35m.

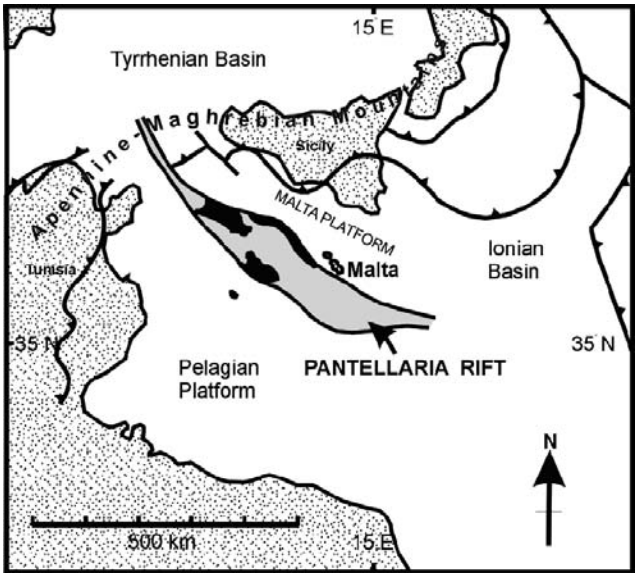

Figure 1 - Bonson et al.

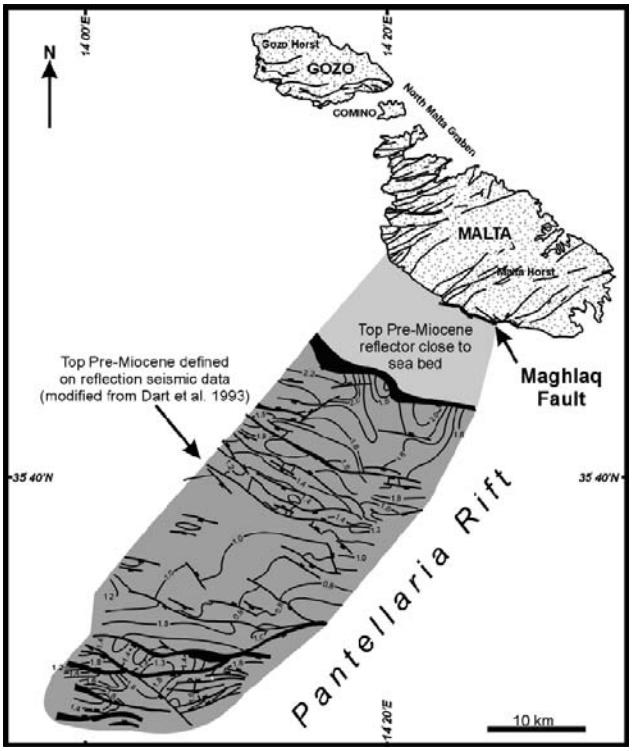

Figure 2 - Bonson et al.

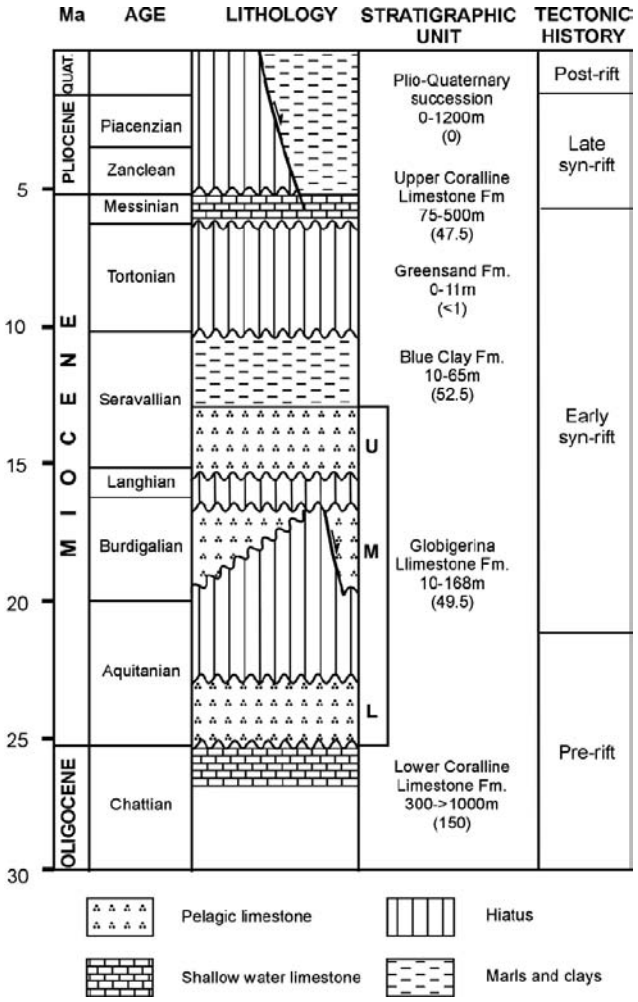

Figure 3 - Bonson et al.

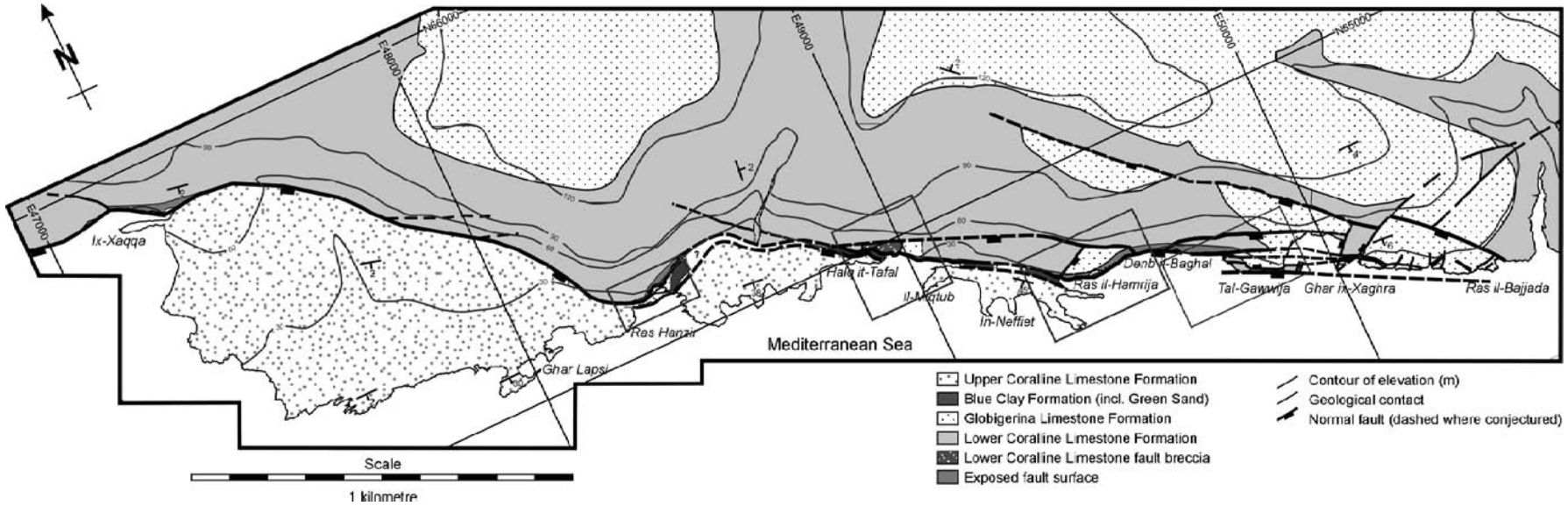

Figure 4 - Bonson et al.

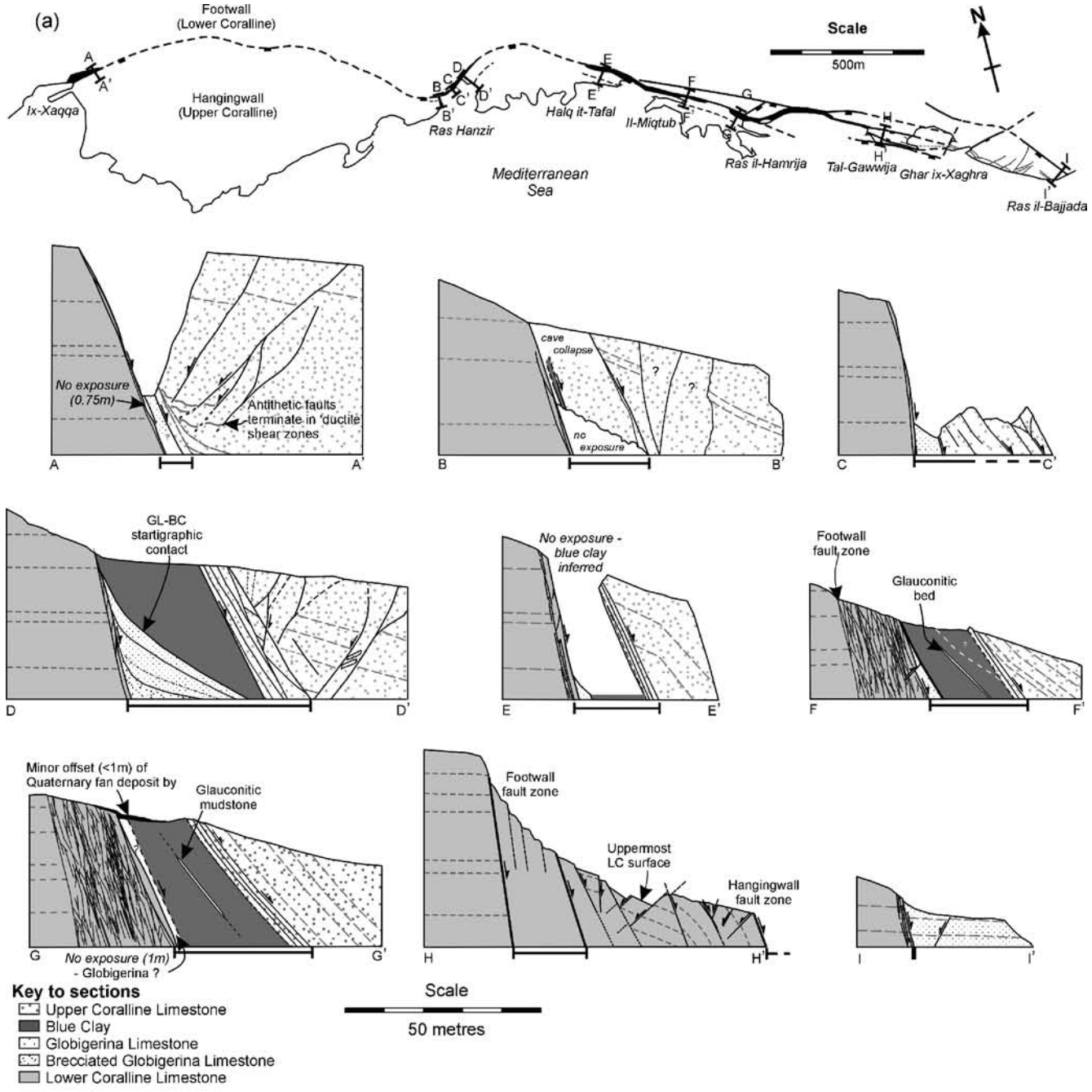

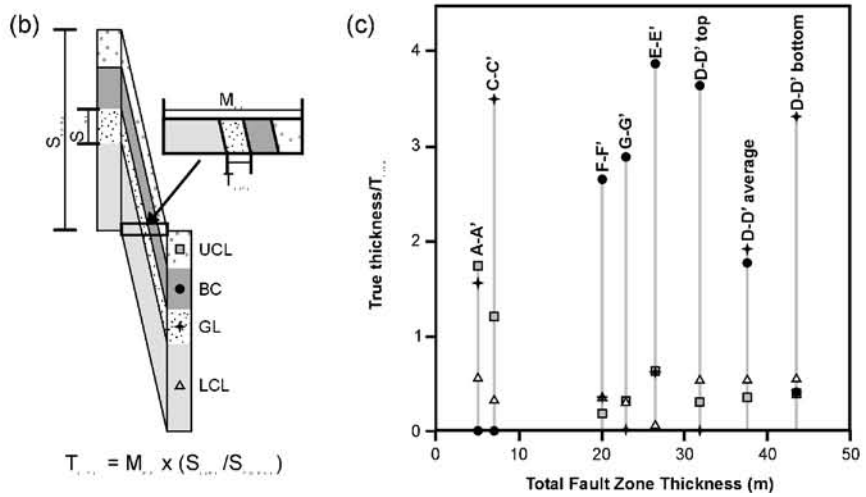

Figure 5 - Bonson et al.

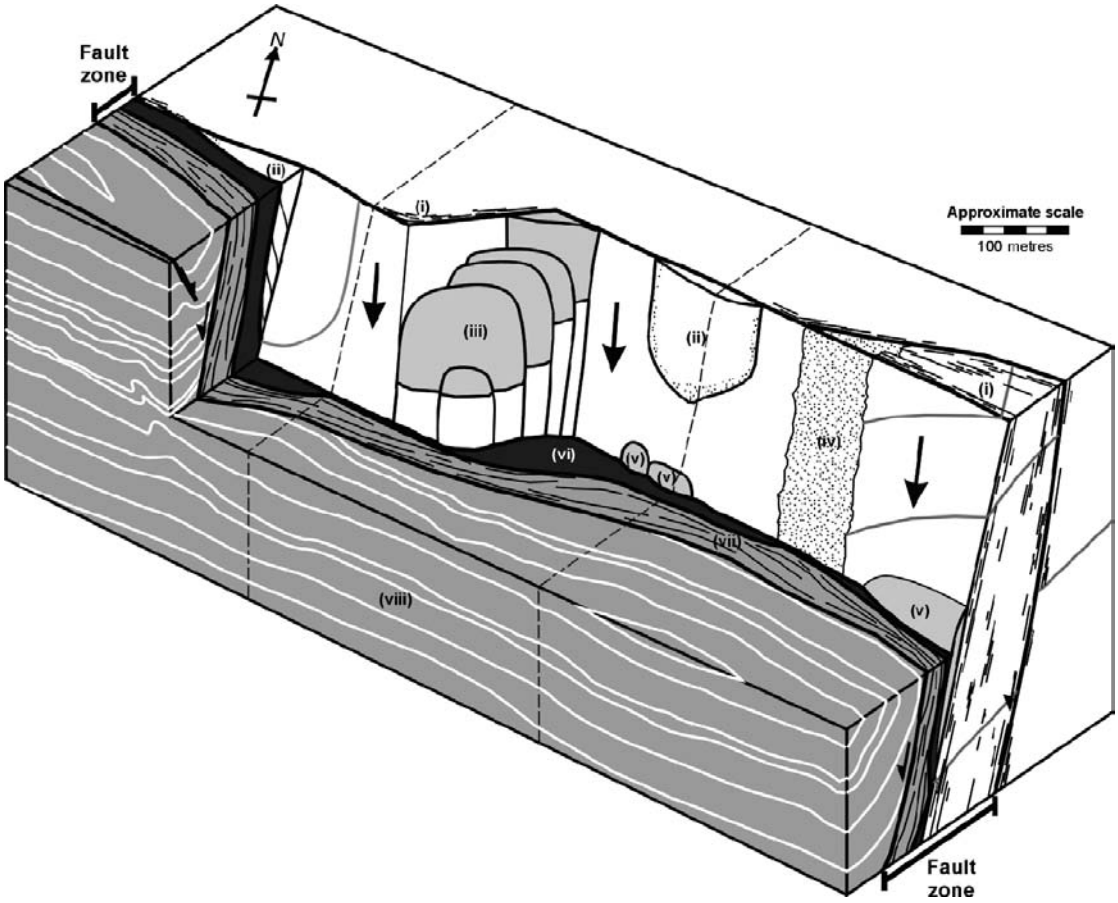

Figure 6 - Bonson et al.

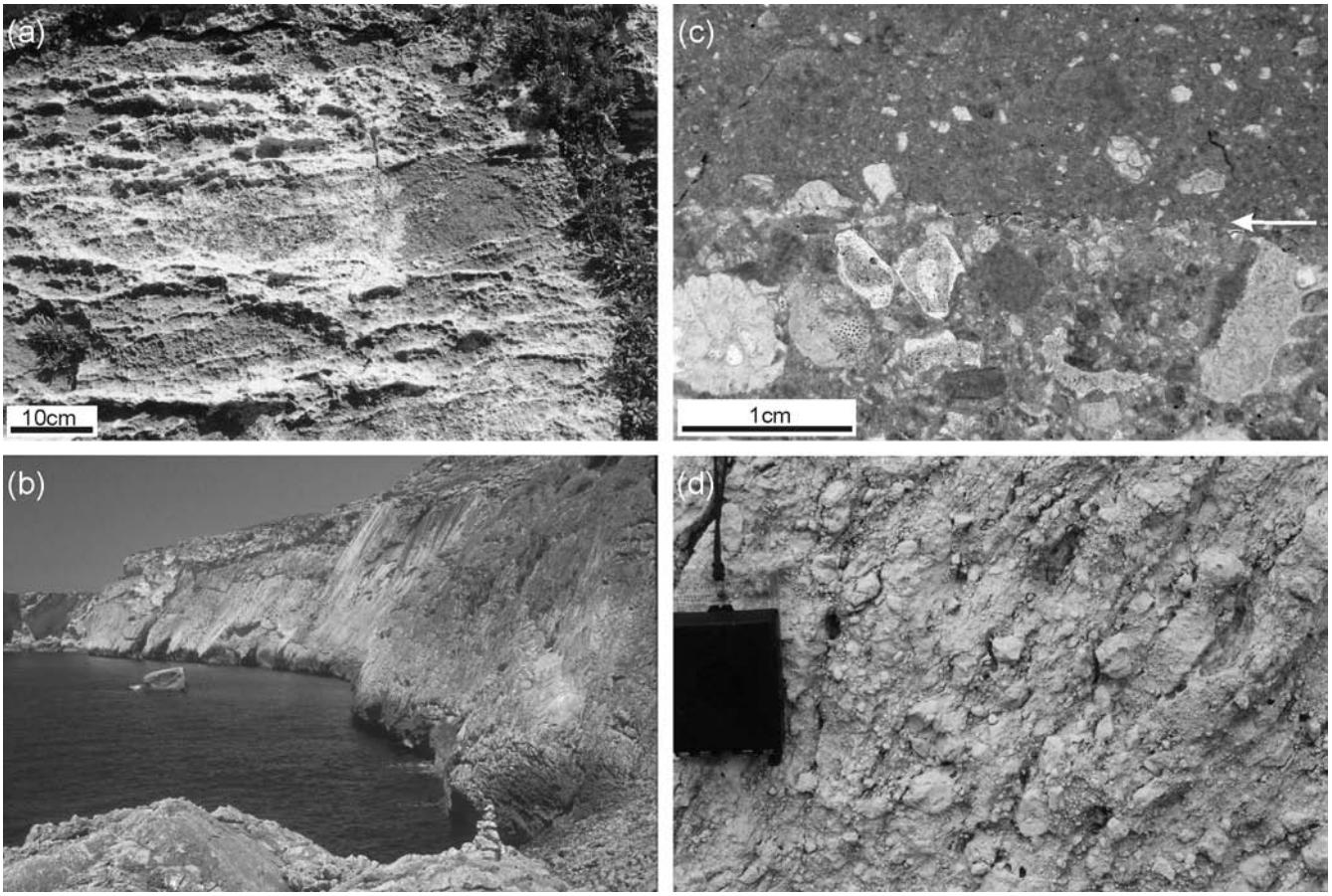

Figure 7 - Bonson et al.

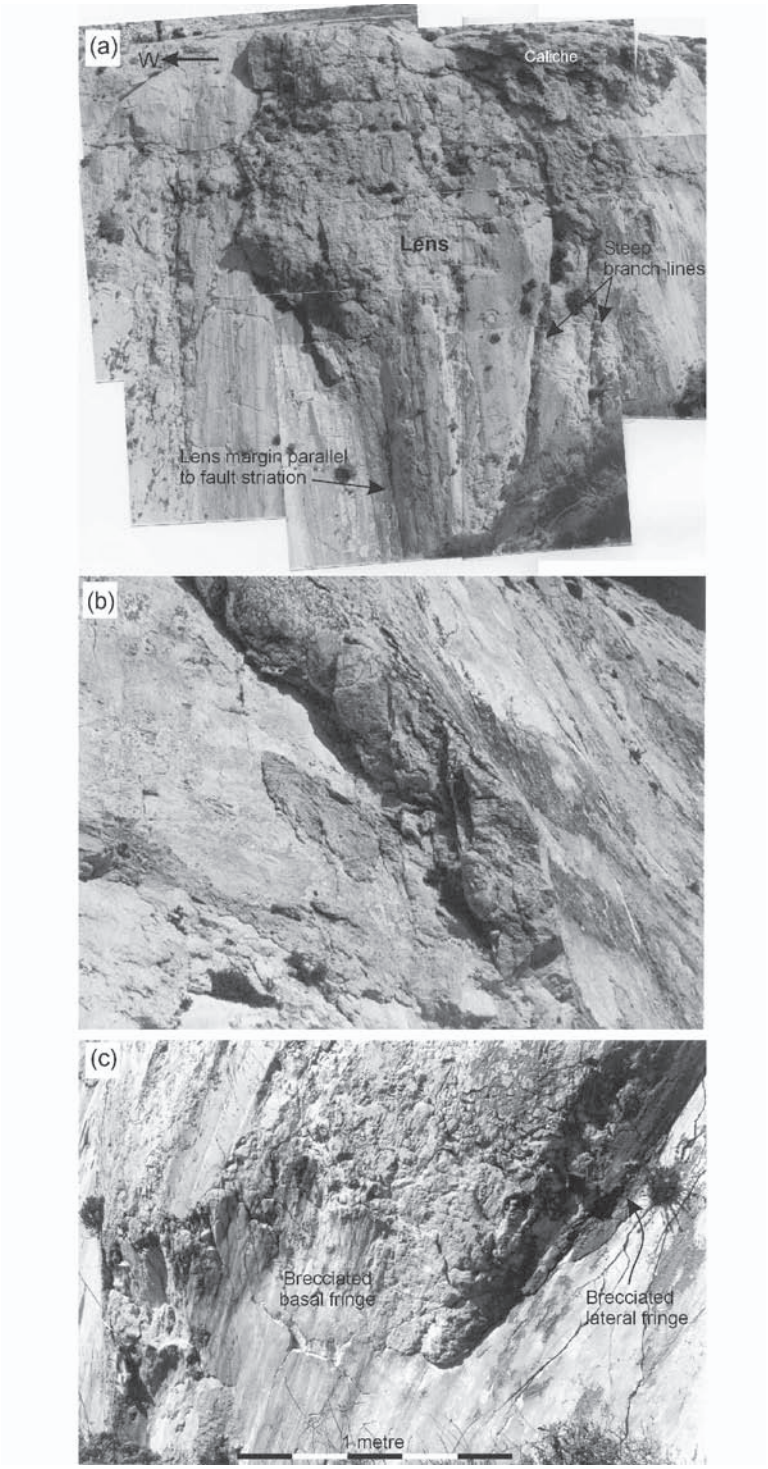

Figure 8 - Bonson et al.

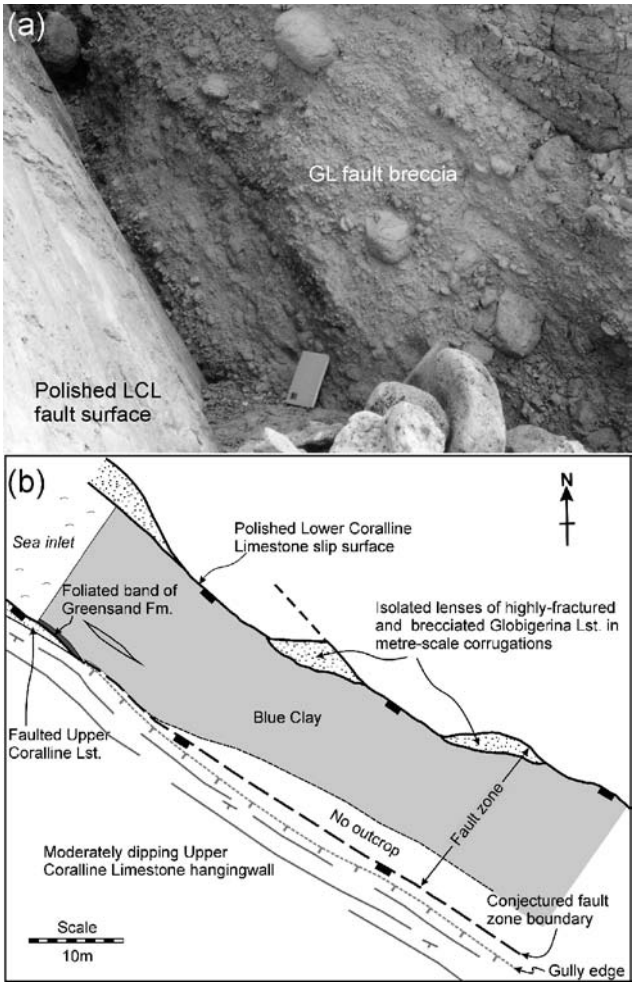

Figure 9 - Bonson et al.

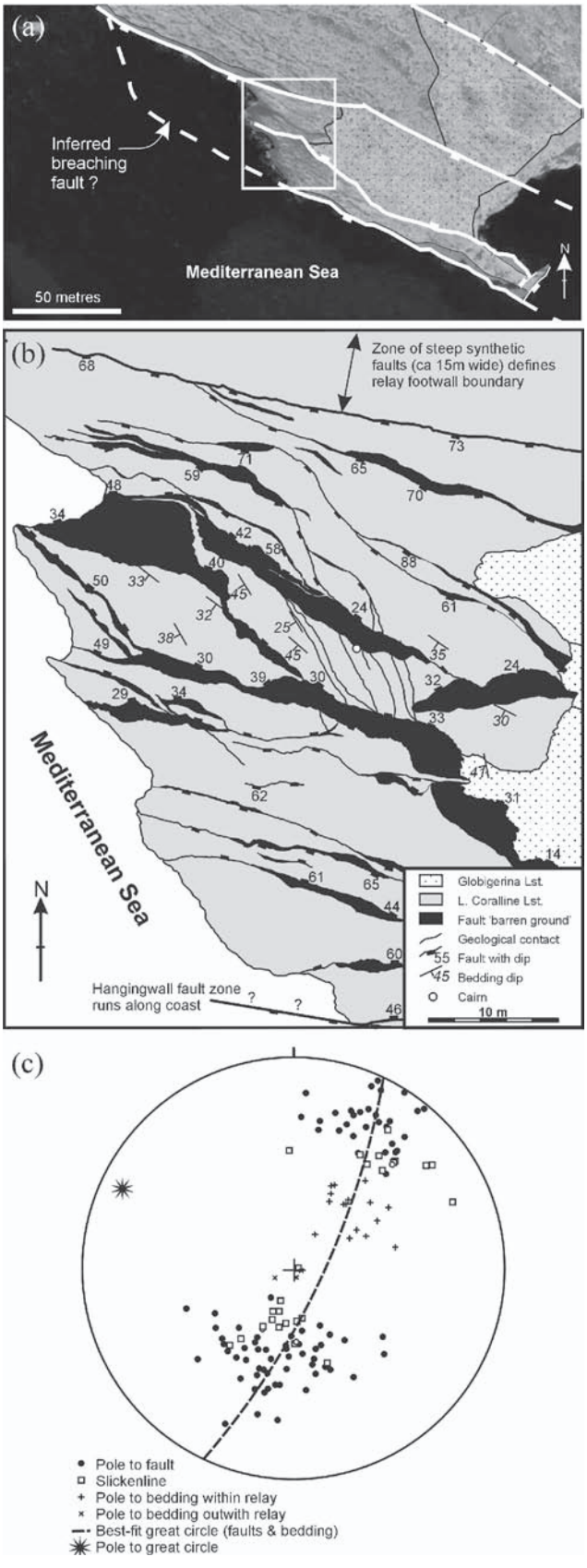

Figure 10 - Bonson et al.

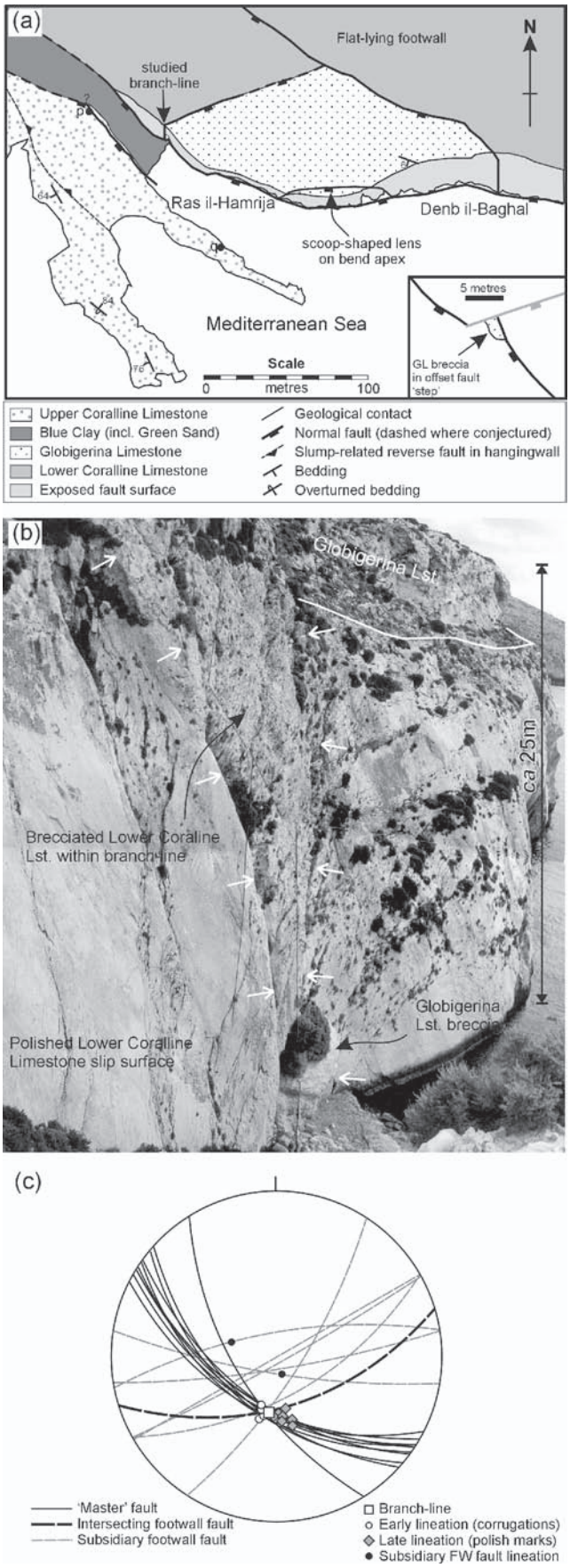

Figure 11 - Bonson et al.

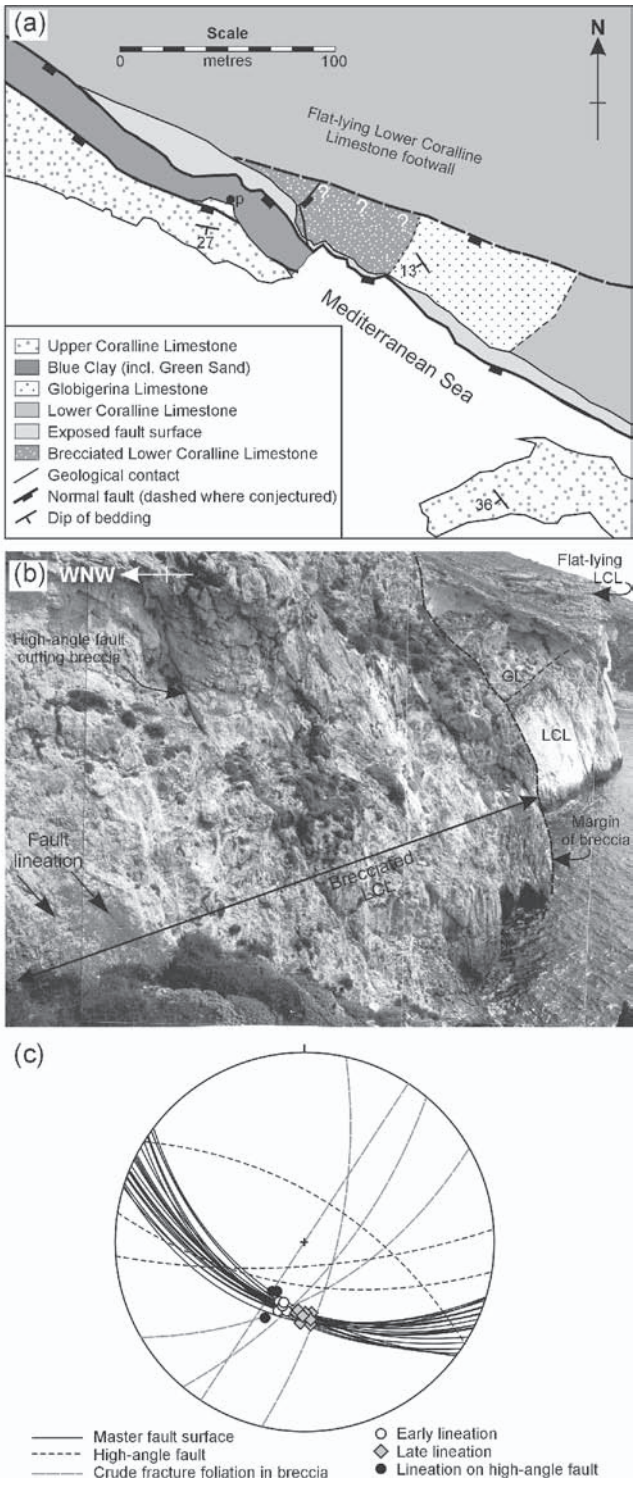

Figure 12 - Bonson et al.

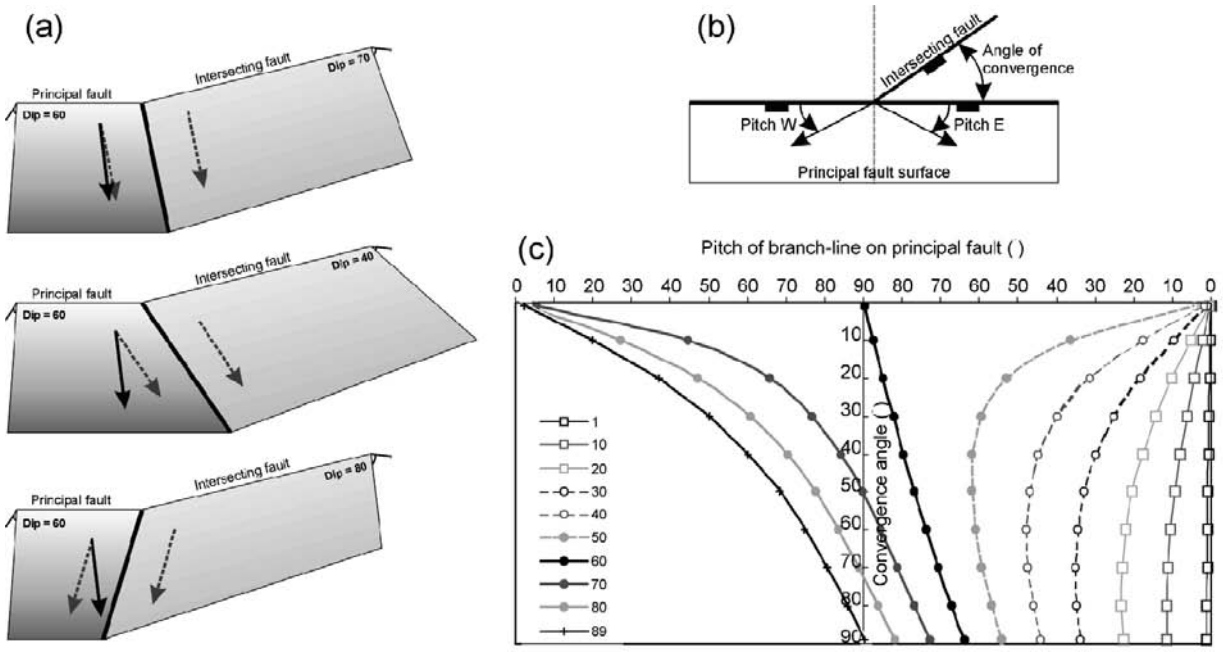

Figure 13 - Bonson et al.

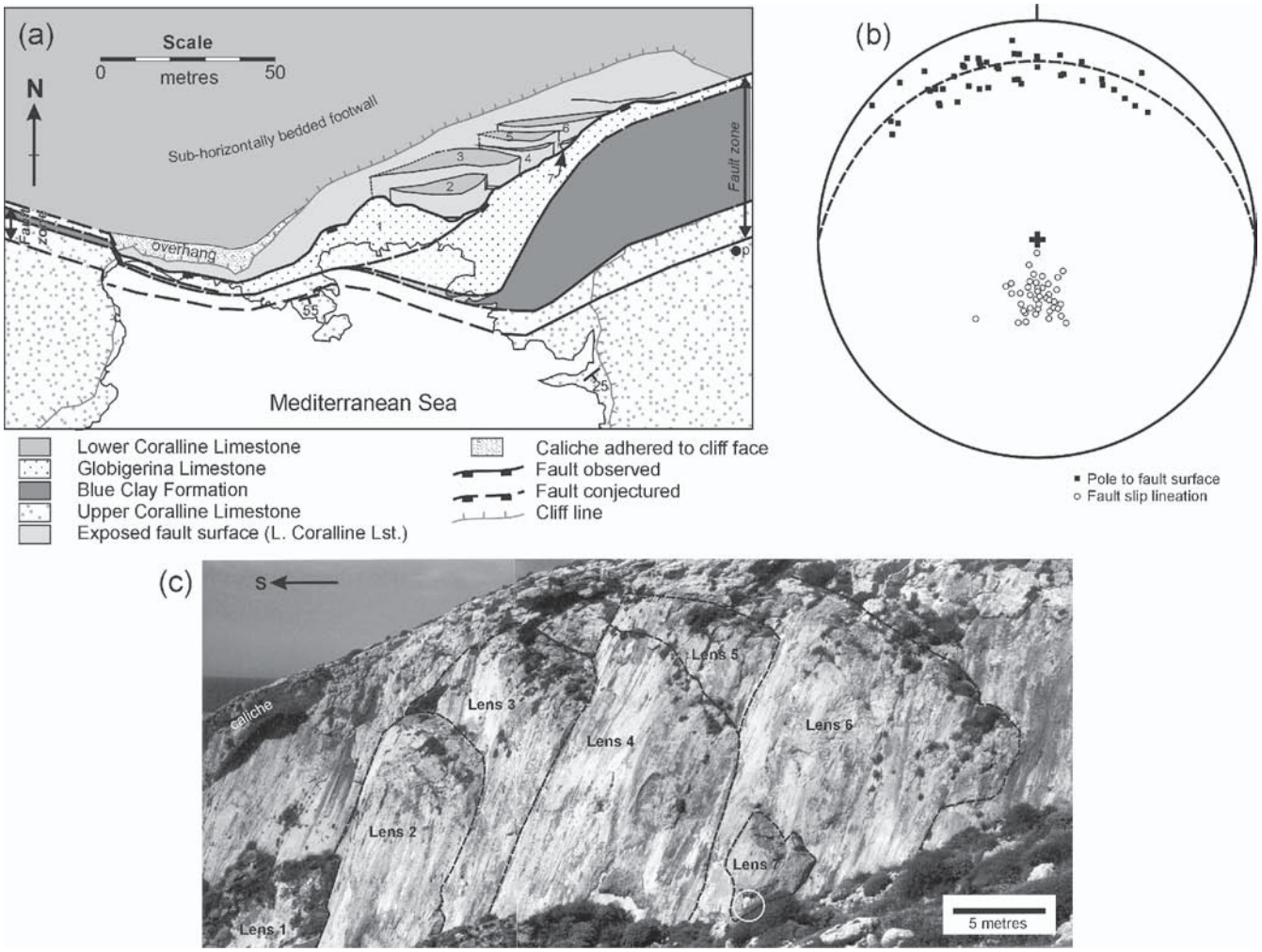

Figure 14 - Bonson et al.

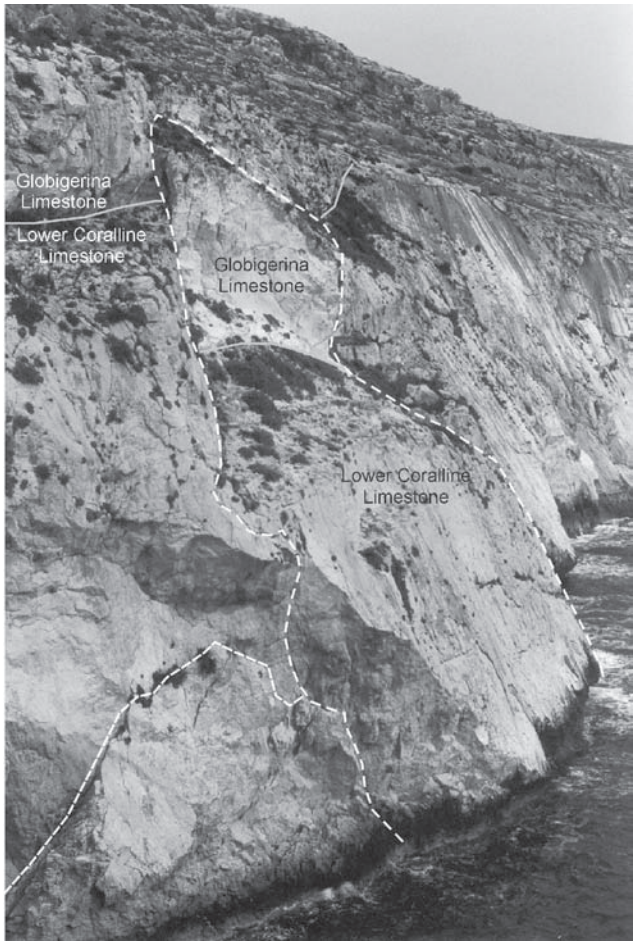

Figure 15 - Bonson et al.